UCL
Université catholique de Louvain

Faculté des Bioingénieurs

Studying the interactions between *Staphylococcus aureus* and atopic dermatitis skin cells using atomic force microscopy

Présenté par Simon Delacroix

Promoteur : Prof. Yves Dufrêne (UCL, ISV)
Co-promotrice : Dr. Cécile Feuillie (UCL, ISV)

Lecteurs : Prof. David Alsteens (UCL, ISV)
Prof. Pascal Hols (UCL, ISV)

Mémoire de fin d'études présenté en vue de l'obtention du diplôme de Bioingénieur :
Chimie et bio-industries

AGRO LOUVAIN
BIOINGÉNIEURS

Année académique 2017-2018

Acknowledgments

Before going into the beautiful world of S. aureus and the AFM technology, it is highly important for me to heartily thank all the persons who enabled me to realize this work that I am proud of.

First I would like to thank Professor Yves Dufrêne for letting me realize this master thesis in his laboratory and for all his advices. I also thank professors T. Foster and J. Geoghegan (Trinity College, Dublin) for the biological equipment provided that was necessary for the experiments that I realized.

I sincerely want to thank Dr. Cécile Feuillie without whom this work would have never been "Great". Many thanks for her patience and her availability to answer my numerous questions. Thanks also for all her advices and all the reviews.

Thanks to my master thesis colleagues; Jérôme and Grégoire for the interesting exchanges and for their happy company.

I also thank all the members of the laboratory for their cheerfulness and their help. I will always (try to) remember that night out with all of them. I wish them good luck for their career and a lot of success in their research.

Last but not least, many thanks to Sophie for her reviews and her unconditional support, to my parents for the enriching discussions that helped me to ask myself the good questions and to all my relatives for their support.

Simon Delacroix

Contents

List of Figures

List of Tables

List of abbreviations

aa Amino acid

AFM Atomic Force Microscope

$CDSN$ Corneodesmosin

Clf Clumping factor

Cna Collagen adhesin

DLL Dock lock and latch

$DMSO$ Dimethyl sulfoxide

ECM Extracellular matrix

EDC 1-ethyl-3-(3-dimethylaminopropyl)- carbodiimide

FD Force-distance

Fg Fibrinogen

FLG Filaggrin gene

$IsdA$ Iron regulated surface determinant A

$K10$ Cytokeratin 10

LR Loading rates

$MRSA$ Methicillin resistant *S. aureus*

$MSCRAMMs$ Microbial Surface Components Recognizing Adhesive Matrix Molecules

NHS N-hydroxysuccinimide

NMF Natural moisturizing factors

OD Optical density

$PAMP$ Pathogen associated molecular patterns

PBS Phosphate buffer saline

PCA Pyrrolidone carboxylic acid

pN pico Newton

PRR Pattern recognition receptors

S.aureus *Staphylococcus aureus*

s.d. Standard deviation

SAMs Self-assembled monolayers

SC *Stratum corneum*

SCFS Single cells force spectroscopy

Sdr Serine aspartate repeat

SdrG Serine–aspartate repeat-containing protein G

SEM Scanning Electron Microscopy

SMFS Single molecule force spectroscopy

SrtA Sortase A

STM Scanning tunnel microscope

TBS Tris Buffer Saline

TLR Toll-like receptors

TSB Trypticase soy broth

VP Vilous protrusions

WT Wild type

WTA Wall teichoic acid

AD Atopic dermatitis

FnBP Fibronectin binding protein

Chapter 1

Introduction

1.1 Atomic Force Microscopy

1.1.1 General features

The Atomic Force Microscope (AFM) technology has been introduced by Binnig et al. (1986) to enable the study of materials and biological systems. This technology is an evolution of the scanning tunnel microscope (STM).

The STM technology consists in scanning a surface with a metal conductive tip at constant tunnel current (Binnig et al., 1982). The displacement of the tip gives a topographic picture of the surface because the height of the tip is constantly adjusted as a function of the tunneling current measured. This current comes from the fact that a charged surface will have some free electrons that go over the surface and if the tip is close enough, a really weak current can be measured between the tip and the surface. This technique presents 2 major limitations: the surface has to be conductive in order to be imaged and the experiment has to be carried out under a high vacuum. This technique alone is thus ill-suited to the study of biological systems.

AFM doesn't rely on tunneling current anymore, but still involves scanning the surface of a sample with a sharp tip mounted on a soft cantilever in order to image it and study its properties. The principle of AFM is described in Figure 1.1.

A laser beam is reflected on the extremity of the cantilever onto a photodiode (Fig. 1.1) as the cantilever is scanning the surface of a sample. Depending on the sample's topography and the interactions between the sample and the tip, the cantilever is attracted or repulsed from the surface. The deflection is monitored by the reflection of the laser on the surface of the cantilever in the photodiode. A piezo electric scanner placed either in the AFM head or under the sample controls the movements of the cantilever or the sample in the scale of the nanometer.

The cantilever has to fulfill two necessary conditions (Binnig et al., 1986):

- It has to be as light as possible. If the cantilever is too heavy, the force required to move it across the sample will mask any force of interaction between the cantilever and the sample.
- It has to be really soft in order to have a maximum deflection for a given force.

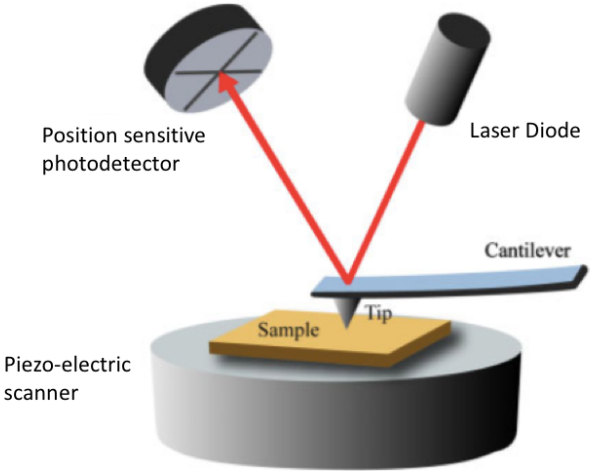

Figure 1.1: **Principle of Atomic Force Microscopy.** A sample is placed over a piezoelectric scanner. A cantilever equipped with a sharp tip scans the sample, and the positive and negative deflections of the cantilever are measured by the reflection of a laser on the cantilever into a position-sensitive photodetector (adapted from Liu and Wang (2010)).

The cantilever will act as a spring near the surface of the sample. Its movements can be described by Hooke's Law :

$$F = k.d \tag{1.1}$$

where k is the spring constant of the cantilever and d the displacement of the laser beam on the photodiode, thus linking the force between the tip and the sample to the deflection of the cantilever. The forces of interaction between the sample and the tip are measured with a pico Newton (pN) precision by the AFM technology.This is crucial, as it enables the analysis of relevant samples at inter-atomic scale.

Imaging modes

The first imaging mode is the contact mode (Fig. 1.2), where the tip is in constant contact with the sample. The force applied to the surface is kept constant by continualy adjusting the height of the cantilever through a retroaction loop. The result is a topographic map of the sample. The resolution depends on the structure of the AFM tips, the sample roughness, the physical properties of the sample and the precision of the feedback loop of the piezo-scanner (Dufrêne et al., 2017). This method is however limited by the delicate adjustment of the force applied to the sample to keep its surface intact.

The tapping mode, or dynamic mode (Fig. 1.2), has been developed in order to minimize the friction between the tip and the sample (Dufrêne et al., 2017). By reducing the lateral forces, the tapping mode allows the study of biological systems that are poorly adsorbed on the surface or objects that are rougher (Dufrêne et al., 2017). In this case, the cantilever is driven at a constant frequency near resonance and the force variations can be detected either as a variation in the amplitude or in the phase of the cantilever vibration (Albrecht et al., 1991).

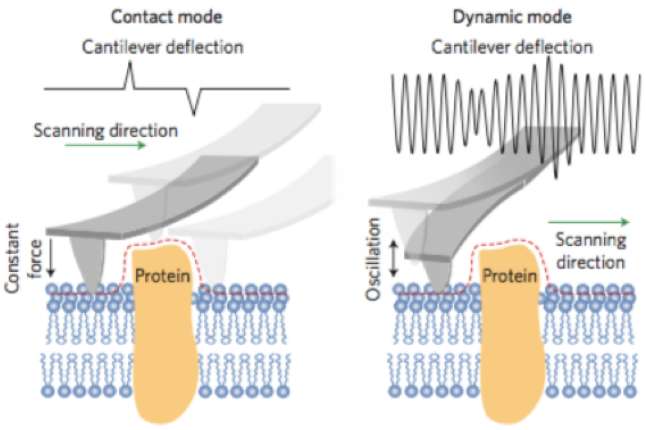

Figure 1.2: **Principle of two imaging modes in AFM.** The contact mode (Left) consists of a constant force applied to the sample; any topographic change modifies the cantilever deflection and the tip-sample distance is constantly adapted by a retro-action loop. The Dynamic mode (right) consists of an oscillation of the cantilever at or near its resonance frequency over the sample and any variation of the sample topography modifies the oscillation leading to an adjustment of the tip-sample distance (Dufrêne et al., 2017).

Force spectroscopy modes

The AFM can also be used to measure the interaction between a sample and the cantilever, represented by force vs displacement curves. A force curve is obtained by monitoring the deflection of the cantilever as a function of the vertical displacement of the piezoelectric scanner, while the cantilever performs approach-retract cycles from the surface. These data give information such as forces of interaction between the tip and the sample and adhesion energy (Gaboriaud and Dufrêne, 2007). The procedure to obtain these force curves is illustrated in Figure 1.3 and

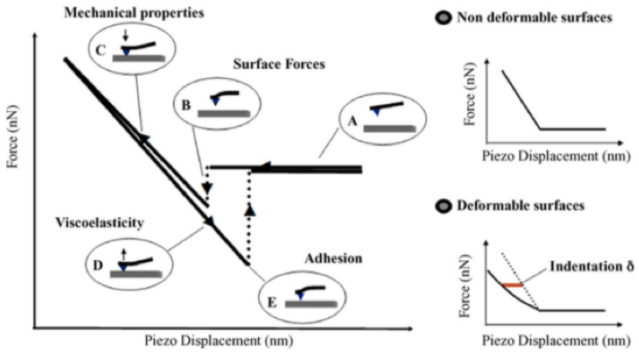

Figure 1.3: **Representation of a typical force-distance curve** for a non deformable surface (Left) with the different stages of the approach (A,B,C) and the retract phase (D,E). Differences between force-distance curve for non-deformable surfaces and deformable surfaces (right) (Gaboriaud and Dufrêne, 2007).

can be described with the following steps: first, the cantilever is lowered towards the surface of the sample (Fig. 1.3A) and in some cases, the cantilever will bend downwards due to van der Waals interactions (Fig. 1.3B). Second, the tip enters in contact with the surface and the tip bends upwards until a pre-defined setpoint of vertical deflection is reached (Fig. 1.3C). Third, the cantilever moves away from the surface and in case of adhesion, there is a hysteresis in

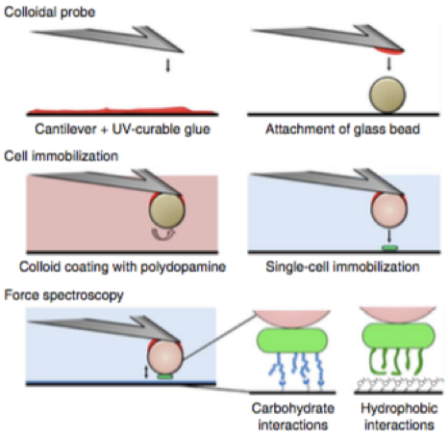

Figure 1.4: **Single cell force spectroscopy protocol**, which consists of the attachment of a glass bead to the cantilever by the use of UV-curable glue, then a colloidal coating with polydopamine and a single-cell immobilization by interaction between the cell and the polydopamine. The interactions between the cell and a sample of interest can then be measured (Beaussart et al., 2014).

the curve corresponding to the adhesion force (Fig. 1.3E) which depends on the interaction between the sample and the cantilever (Gaboriaud and Dufrêne, 2007). The first two steps constitute the approach and the last ones the retraction curve. The shape of the curve will also depend on the deformability of the surface. When the surface is deformable / soft, we observe an indentation (Fig. 1.3, right) (Gaboriaud and Dufrêne, 2007).

Raw data for a force curve consists of voltage / displacement curves, that need to be converted into forces / displacement curves. Two intrinsic parameters of the AFM tip are needed, its sensitivity and its spring constant. The sensitivity S, in m/V, is the slope of the retraction curve when the sample and the cantilever are in contact, and allows converting the observed voltage deflection on the photodiode in Volt (V) into the cantilever deflection in meter (m). The spring constant K, in N/m, allows the transformation of the cantilever deflection into forces by Hooke's law (Eq. 1.1) (Hinterdorfer and Dufrêne, 2006).

Single cells force spectroscopy (SCFS) It is possible to functionalize the cantilever with a living cell, allowing the direct measurement between a live cell and a surface. In this method called single cell force spectroscopy (SCFS), a single cell of interest is immobilized on the cantilever. For the fixation of the cells, different methods are used such as receptor ligand interactions, electrostatic interactions, glue or chemical fixation (Hinterdorfer and Dufrêne, 2006). It is important to be sure that the metabolic activity and the natural surface architecture of the cells are preserved and also to control the number of cells that will interact (Dufrêne, 2015).

One fixation method is to use a colloidal silica bead fixed at the apex of a tip-less cantilever and further coated with polydopamine (Fig. 1.4). A single cell is then immobilized by putting the silica bead in contact with the cell (Beaussart et al., 2014). This method is nondestructive and offers a good control of the contact area, which gives the possibility of reproducible single cell analysis (Dufrêne, 2015).

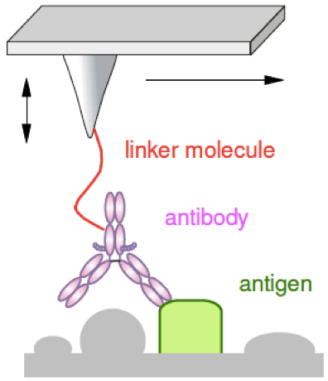

Figure 1.5: **Principle of single molecule force spectroscopy** applied to antibody – antigen interactions. The Cantilever is functionalized with a protein of interest, here an antibody, separated from the tip by a linker molecule. The antibody will interact with the antigen / specific receptor on the sample, resulting in a force that will be measured by AFM. (adapted from Ebner et al. (2007))

Single molecule force spectroscopy (SMFS) In single molecule force spectroscopy (SMFS), the cantilever is functionalized with a molecule of interest and the interactions between this specific molecule and the sample will be measured. This principle is illustrated by Fig. 1.5.

Several factors have to be considered to achieve optimal detection. (i) The binding of the molecule on the tip has to be much stronger than the molecular force studied. Covalent bonds are the best way to achieve this because they are stronger than typical receptor-ligand bonds. (ii) The density of grafted molecules on the cantilever has to be low to ensure single molecule interactions. (iii) The use of a flexible molecular spacer allows the molecule to freely interact. (iv) It is also important to limit nonspecific interaction. (v) The orientation of the molecule can be important and can be controlled in some cases: for instance, if the protein has a histidine tag, it is possible to use it to anchor the protein through $NTA - Ni^{2+} - His$ bonding (Hinterdorfer and Dufrêne, 2006). The biomolecules can be attached on a gold-coated cantilever via self-assembled monolayers (SAMs) of functionalized alkane thiols. The end-groups of the alkane thiols will react with the biomolecule of interest. Commonly, two types of thiols are used, one with a hydroxyl functional group and one with a carboxyl functional group. Carboxyl groups are activated with a solution of NHS/EDC (N-hydroxysuccinimide (NHS); 1-ethyl-3-(3-dimethylaminopropyl)- carbodiimide (EDC)) and will be able to form covalent bonds with the amine groups of the aimed protein (Ebner et al., 2007). The use of a linker between the tip and the molecule allows to easily separate the specific interactions from the non-specific ones.

Force-distance (FD) based AFM imaging

It is possible to image a biological system and simultaneously map the properties of the system at a molecular resolution by using Force-Distance (FD) based AFM, or multiparametric imaging (Fig. 1.6). The AFM records FD curves over the sample and maps the interactions pixel by pixel at angstrom precision and piconewton sensitivity. Eventually the interactions can be correlated to the topography of the sample (Dufrêne et al., 2013).

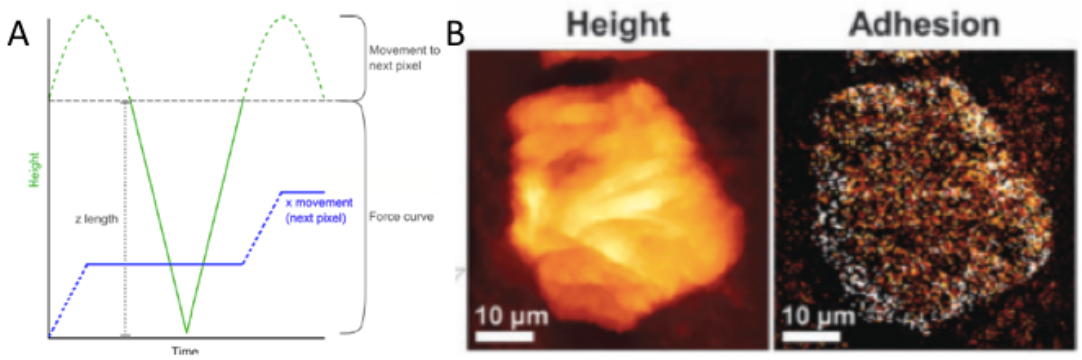

Figure 1.6: **FD-based AFM.** Displacement of the AFM tip in QI^{TM} mode (JPK, 2011) (A). Image of Height and Adhesion obtained by QI^{TM} mode (B). For each pixel of the image, a force-distance curve is recorded (adapted from Formosa-Dague et al. (2016)).

1.2 *Staphylococcus aureus*

1.2.1 Health issues

Staphylococcus aureus (*S. aureus*) is a commensal gram positive bacterium belonging to the order of Bacillales and the family of Sthaphylococcacae. In greek, "staphylé" means "a bunch of grapes". On the Scanning Electron Microscopy (SEM) image presented on Figure 1.7 we can see that *S. aureus* has a round shape and tends to gather in small groups. *S. aureus* is a non-motile and non-spore forming bacterium. They are also facultative anaerobes but grow better in aerobic conditions. Compared to other staphylococci, *S. aureus* has the unique particularity to present clumping factors and coagulase. Finally *S. aureus* carries more than 20 adhesin genes (Foster et al., 2013) but we will focus on only 3 of these adhesins in this study.

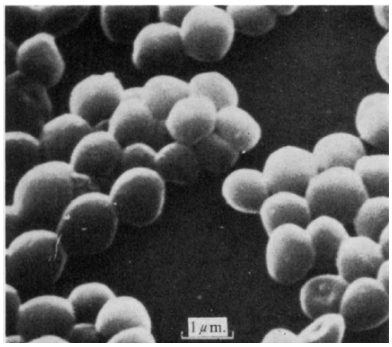

Figure 1.7: **SEM image of *S. aureus*** during the logarithmic growth phase (Greenwood and O'Grady, 1972).

This bacterium is colonizing the skin and the nose of humans. The population is colonized differently: 20% of the human population is persistent carriers, then 30% is intermittent carriers and finnaly, 50% is non carriers (van Belkum et al., 2009). *S. aureus* can be pathogenic (van Belkum et al., 2009) and is involved in different disorders such as endocarditis or skin infections. Throughout this work we will mainly focus on skin infections and more especially on Atopic dermatitis (AD) knowing that 75 to 100% of patients who suffer from AD present *S. aureus* on their lesioned skin (Park et al., 2013).

The *S. aureus* bacteria, such as the methicillin resistant *S. aureus* (MRSA), are found to be more and more resistant to antibiotics (Foster et al., 2013). MRSA can practically resist any existing antibiotic, which has made it a rising health threat for the last 3 decades (Que and Moreillon, 2014). The emergence of this antibiotic resistance was not a surprise since in 1944 resistance to penicillin was already observed. After Alexander Fleming received his Nobel price, he said "The thoughtless person playing with penicillin treatment is morally responsible for the death of the man who succumbs to infection with the penicillin-resistant organism". Bacteria are really versatile and they can easily develop resistance. Moreover, *S. aureus* is known to form biofilms in three steps: adhesion, maturation and detachment. Within a biofilm, bacteria are even more resistant to antibiotic treatment (Jørgensen et al., 2016). It is thus important to develop other mechanisms to fight those infections. So if it is no longer possible to treat *S. aureus* infections with the help of antibiotics, an alternative strategy can be to target the mechanism of this biofilm formation in order to get rid of the nosocomial infection. In this work we will study the mechanism of the adhesion of *S. aureus* onto human skin affected by AD, in order to know which skin ligands and which adhesion proteins of *S. aureus* are responsible and can be a target for anti-adhesive strategies.

1.2.2 The adhesins

Adhesion proteins of *S. aureus*, or adhesins, are covalently anchored to the cell wall of the bacteria (Foster et al., 2013) , which is made of 50% of peptidoglycan by weight for *S. aureus*. The main enzyme responsible for the adhesion is the sortase A (SrtA). SrtA is essential for the expression of the adhesins on the surface of *S. aureus* (Mazmanian, 1999). The expression of the adhesins on the surface can vary between stationary and exponential growth phase. (O'Brien et al., 2002). The adhesins confer the ability to *S. aureus* to adhere to extracellular matrix (ECM) and ensure its colonization throughout the host, which constitutes the initial step in the infective process (O'Brien et al., 2002). The largest group of adhesins, called Microbial Surface Components Recognizing Adhesive Matrix Molecules (MSCRAMMs), gathers a family of proteins similar by their structure (Fig. 1.8). In the MSCRAMMs family we can distinguish 3 sub-categories: the Clumping factor-Serine aspartate repeat (Clf-sdr), the Fibronectin binding proteins (FnBPs) and the Collagen adhesin (Cna) protein family. In this work we will focus on The Clf-sdr and the FnBPs families of protein which are presented in Figure 1.8. As we can see on Figure 1.8, all MSCRAMMS present first a signal sequence at the N terminal region and a sorting signal at the carboxyl terminus. Between these two signals we can observe an A region with N1 N2 and N3 sub-domains, and a R region containing repeated groups. The R domain differs by the repeat group, which is Serine aspartate for the Clf-Sdr, and Fibronectin binding repeats for FnBPs (Foster et al., 2013).

MSCRAMMS are also characterized by similar mechanisms of binding to ligands. A mechanism known as the dock, lock and latch (DLL) mechanism is mediated by two adjacent IgG like subdomains, localized in the N terminal A region and corresponding to the N2 and N3 domains of Figure 1.8 (Foster et al., 2013). This mechanism has been described by (Ponnuraj et al., 2003). Figure 1.9 illustrates one variant of the DLL, showing serine–aspartate repeat-containing

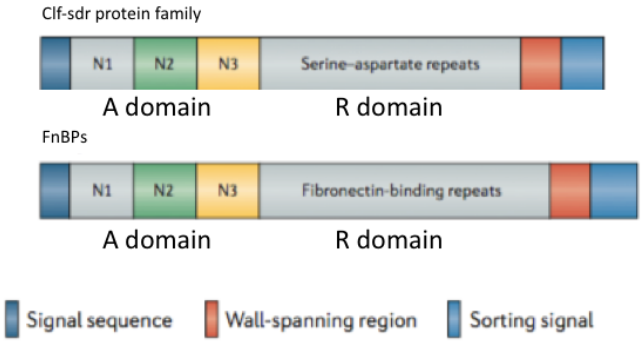

Figure 1.8: **Structural motif of MSCRAMMs adhesins Clf and FnBPs**. MSCRAMMS are characterized by a signal sequence at the amino-terminus, a sorting signal at the carboxy-terminus, and a wall-spanning region, where the protein is anchored into the cell wall. The remaining structure is then separated in two domains, A and R domains. The A domain is composed of three separately folded subdomains N1, N2, N3; the N1 and N2 subdomains form igG like folds which binds ligands by the Dock lock and latch (DLL) mechanism (Adapted from Foster et al. (2013)).

protein G (SdrG) binding to Fibrinogen (Fg). A trench can be observed between the N2 and N3 domain, where the ligand will dock. This docking will induce a conformational change within the N3 domain were the G' strand will go over the trench and lock the ligand in place. Finally, The G" strand will be inserted between the strands E and D by a complementation of a β sheet in the N2 domain. This final step is called the latch (Ponnuraj et al., 2003).

Previous studies have shown that ClfB and FnBPs are implicated in the adhesion of *S. aureus* to the skin (Fleury et al., 2017; Cho et al., 2001). This is why we chose to focus on three adhesins belonging to the MSCRAMM family, FnBP A and B and clumping factor B (ClfB), which differ by the presence of fibronectin binding repeats or serine-aspartate repeats in their R region.

FnBP A and FnBP B are partly responsible for the adhesion of bacteria cells to fibronectin. Fibronectin is a glycoprotein from the extracellular matrix of the host, which binds to surface receptors integrins. Foster et al. (1999) have shown that there was no difference of adherence if only one of the FnBPs was expressed, but the deletion of both adhesins leads to less adhesion to epithelial cells and no internalization of *S. aureus*.

ClfB is a bifunctional protein that binds to human cytokeratin 10 (K10) and fibrinogen (Fg) (O'Brien et al., 2002). O'Brien et al. (2002) have demonstrated that ClfB is a major determinant in *S. aureus* nasal colonization. It is attached in the cell wall by sortase A. This bacterial protein responsible for the adhesion of *S. aureus* to keratin is more expressed during the exponential phase of growth (O'Brien et al., 2002). Mulcahy et al. (2012) have also demonstrated that ClfB promotes the adherence to immobilized loricrin, another skin protein. Vitry et al. (2017) have shown that the force of this ClfB / loricrin adhesion is consistent with the adhesion mechanism of Dock lock and Latch (DLL).

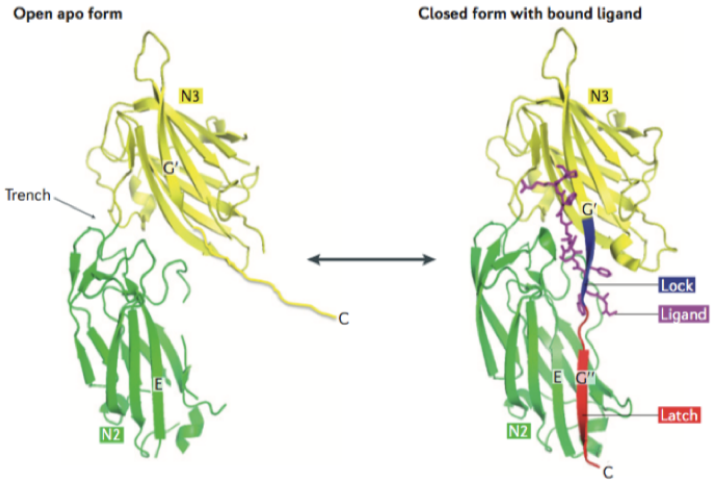

Figure 1.9: **Dock lock and latch mechanism** (DLL). The ligand docks in a trench between the two domains N2 and N3, and is locked by a conformational change of the N3 subdomain. A complementation of the β sheet in the N2 subdomain completes the latch (adapted from Foster et al. (2013)).

1.3 The Human skin

1.3.1 General properties

The human skin is a surface of about 1.8 m^2 where a lot of microorganisms are living in diverse ecosystems. Its first role is to protect, by physical barriers, our body from invasion of pathogens or toxic substances. All microorganisms that are present on the skin are mainly harmless and can also be helpful for the organism for example in the presentation of pathogens to the lymphocyte T (Grice and Segre, 2011).

The skin is made of different layers, represented in Figure 1.10. Located over the derm, the epiderm represents the first barrier to the external environment, and is also composed of several layers. Directly above the derm are the basal, spinous, and granular layers, topped by the most external layer, the corneal layer or *stratum corneum* (SC), which is a cornified layer made of corneocytes and keratinized dead cells and is only present on the epithelium of the skin. The corneal layer is the skin's major physical barrier, and is mainly composed of terminally differentiated keratinocytes, that belong to the most abundant cell type in the epidermis and are devoid of organelles. The keratinocytes migrate through the layers of the epiderm to the corneal layer (Krishna and Miller, 2012).

The Keratinocytes in the epidermis are also known to express pattern recognition receptors (PRR) such as Toll-like receptors (TLR), which recognize pathogen associated molecular patterns (PAMP) from microorganisms (Nestle et al., 2009). Those receptors can also activate an inflammatory path leading to an immune response.

Within the *stratum corneum*, the corneocytes are held together by structures called corneodesmosomes (Fig. 1.11) (Kitajima, 2015), which are adhesive structures made up of complex proteins, including the corneodesmosin (CDSN). This 56 kDa glycoprotein is expressed on the upper surface of the skin, in the granular and the stratified layers of the epidermis (Rankl et al., 2010).

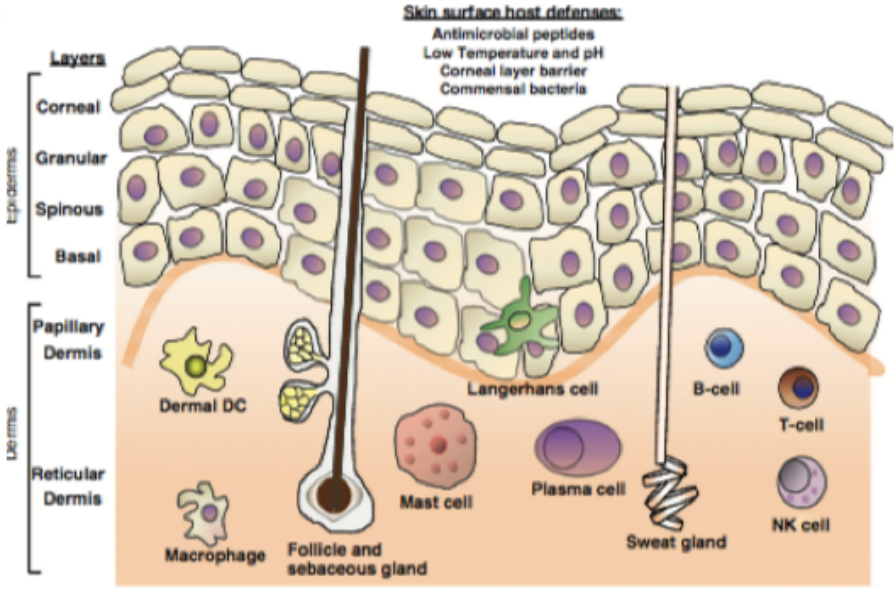

Figure 1.10: **Structure of the human skin** (A) The first defenses of the skin are its constitutive properties such as low temperature and pH, as well as skin commensals and antimicrobial peptides, which resist to *S. aureus* colonization. The first layer of the skin is the epidermis, composed of different sub-layers, which are the corneal, granular, spinous and basal layers. The underlying layer is the dermis composed of two sub-layers, the papillary and the reticular dermis. In the dermis we can find several elements involved in the immunity system (Krishna and Miller, 2012).

The skin is a complex ecosystem where the acidity, the humidity and other factors have to be stable in order to keep a healthy skin. When those factors are disturbed, the skin can be affected by several diseases. As already mentioned, in this work we will mainly focus on one particular skin disease, the Atopic dermatitis (AD) also known as Eczema, a form of skin inflammation. The prevalence of this disease has doubled or tripled in the past three decades in industrialized countries. Worldwide 1 to 3% of children and 2-10% of adults are affected (Bieber, 2008). The disease begins most of the time in early infancy, but can also start at a mature age (Bieber, 2008). One of the first symptoms of AD is the alteration of the *stratum corneum* (*SC*), causing increased trans-epidermal water loss (Bieber, 2008). AD is a genetic disease involving the filament aggregating protein (filaggrin) gene (*FLG*), which is responsible

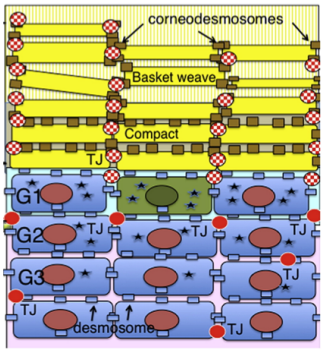

Figure 1.11: **Illustration of the role of the corneodesmosomes in the junction between corneocytes** in the upper layer of the skin (Kitajima, 2015).

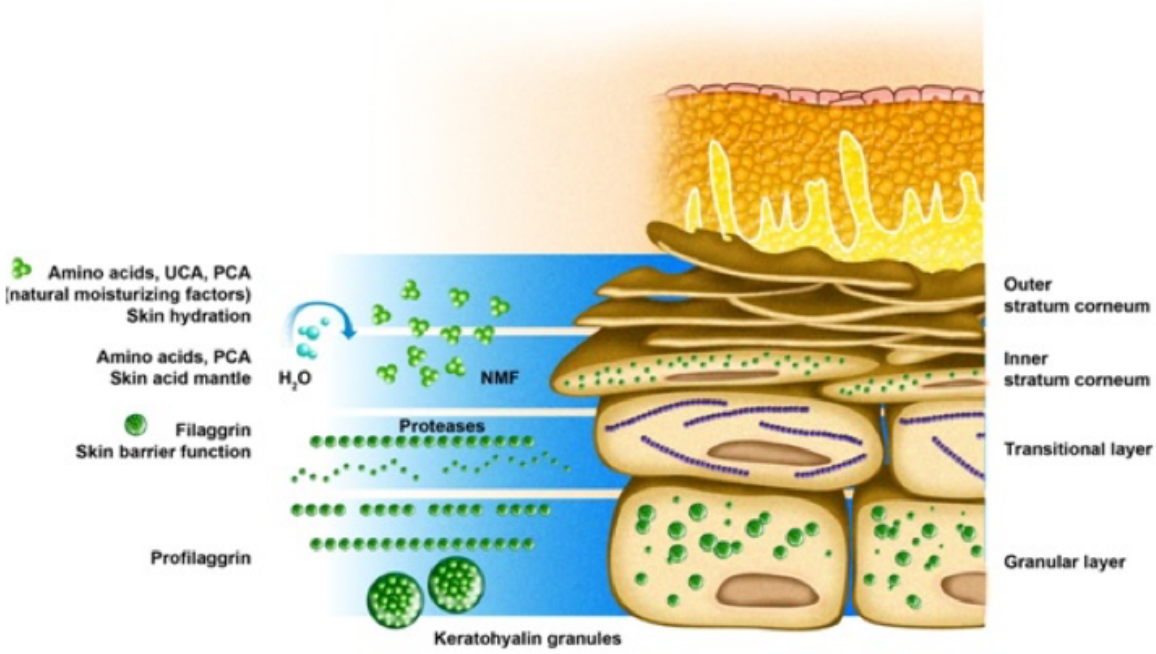

Figure 1.12: **The NMF.** The filagrin is principally found in the outer *stratum corneum*, which is the upper layer of the skin. Filaggrin is the precursor of the natural moisturizing factor (NMF) The caspase 14 enzyme transforms the Filaggrin in free amino acids and pyrrolidone carboxylic acid (PCA), which facilitate the water binding capacity of the skin (O'Regan et al., 2009).

for the regulation of the skin homeostasis and for taking part in skin barrier function (Bieber, 2008). It has been observed that inherited loss of function mutations in the FLG predispose patient to AD (Palmer et al., 2006).

It is therefore crucial to consider an intrinsic factor of the skin: the natural moisturizing factors (NMF)(mmol/g total protein), directly related to the filaggrin protein. The NMF group several components that are together responsible for the water binding in the *stratum corneum* (Fig. 1.12). They are mainly composed of free amino acids, inorganic salts, sugars, lactic acid and urea, all of which are packed within the corneocytes (Fowler, 2012). The NMF play the role of humectants, which bind and attract water from the atmosphere (Fowler, 2012), ensuring proper skin hydration. Analysis of both the NMF components and of the amino acid composition of the SC have shown that these components come from the proteolysis of the filaggrin protein (O'Regan et al., 2009). Even if the corneocytes are nucleus-less, there is still an enzymatic activity, which requires a minimum of hydration to function properly. The NMF are correlated with AD, and it has been shown that AD skins present a reduction of NMF (Kezic et al., 2011).

The presence of *S. aureus* is known to increase the severity of AD by secreting virulence factors such as protein A (TNFα production), α-toxin (lysis of keratinocyte), δ-toxin (mast cell degranulation and inflammation) (Williams and Gallo, 2015). It is therefore important to understand how *S. aureus* interacts with AD skin in order to study solutions against *S. aureus* colonization.

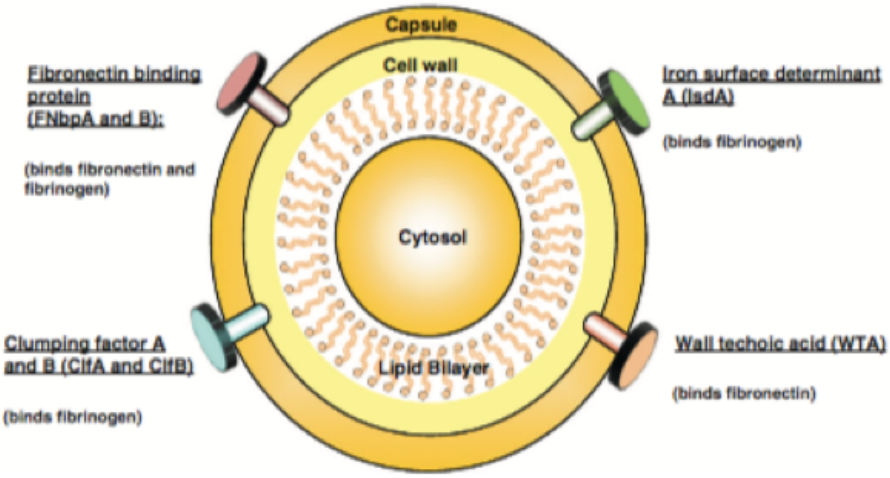

Figure 1.13: **The adherence of *S. aureus* on the skin is mediated by *S. aureus* surface components**, anchored in the capsule and the cell wall, such as fibronectin-binding protein A (FnBP A) and FnBP B, fibrinogen-binding proteins (ClfA and ClfB), iron regulated surface determinant A ($IsdA$) and wall teichoic acid (WTA) (Krishna and Miller, 2012).

1.3.2 Interactions between the skin and *S. aureus*

The adhesins implicated in the adhesion of *S. aureus* to the human skin are illustrated in Figure 1.13; they are FnBP A and B, ClfA and ClfB, IsdA and wall teichoic acid (WTA) (Krishna and Miller, 2012). Previous AFM studies have permited to better undertand the role of some of those adhesins.

The interaction between human skin and *S. aureus* has been previously studied with AFM techniques with healthy skin (Formosa-Dague et al., 2016) and in case of AD (Fleury et al., 2017). ClfB has been identified as a major adhesin involved in *S. aureus* adhesion on AD skin, and the ligand of ClfB is exposed on the *stratum corneum* of the skin of AD patients (Fleury et al., 2017). Indeed, when comparing the adhesion of a *S. aureus* strain expressing ClfB to a mutant strain without ClfB, the adhesion forces measured by AFM were significantly reduced but not totally (Fig. 1.14) (Fleury et al., 2017), which shows that even if ClfB is a major adhesin, other adhesin are implicated in this process of adhesion. For ClfB, the ligand has been identified to be loricrin (Mulcahy et al., 2012) and the interaction has been characterized as a Dock lock and latch interaction thanks to the measured force of interaction (1500 pN)(Vitry et al., 2017). Adhesion of *S. aureus* is stronger on low NMF skins ($\sim$ 1500 pN) compared to high NMF skins ($\sim 50 - 250$ pN)(Fig. 1.14 C, D) (Feuillie et al., Submitted). Low NMF skins are characterized structurally by the presence of vilous protrusions (VP), as shown in Fig. 1.14 E. High NMF skins do present some VP, but much less (Fig. 1.14 F) (Feuillie et al., Submitted). They also highlighted that physical stress potentiates bacterial-corneocyte adhesion by measuring loading rates (variation of the adhesion forces as a function of the rate at which force is applied) (LR), low LR gives forces of $\sim$ 150 pN high LR gives forces of $\sim$ 1500 pN (Feuillie et al., Submitted).

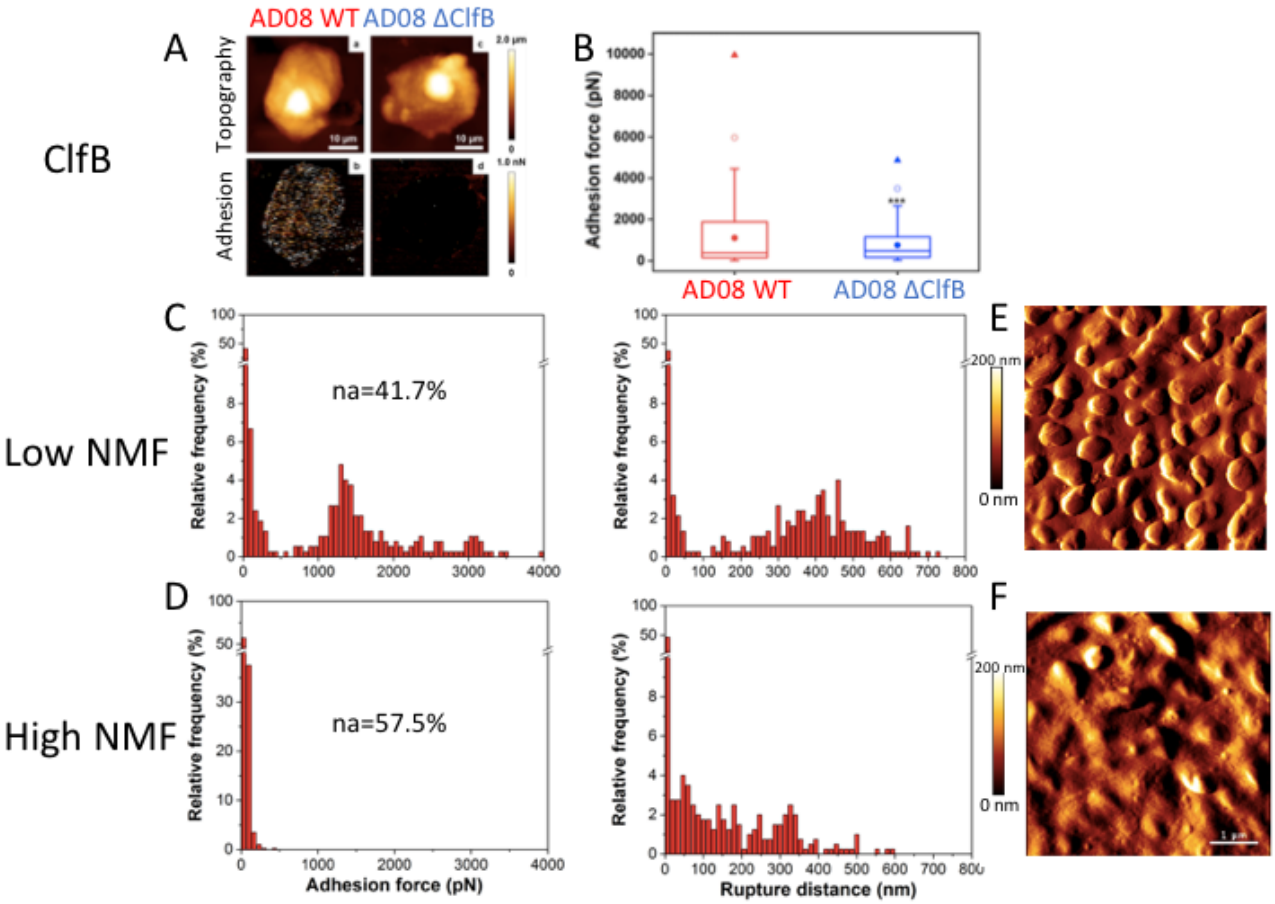

Figure 1.14: **AFM analysis of the skin-*S. aureus* interaction.** (A) QI^{TM} image of the topography and the adhesion of *S. aureus* AD08 Wild type (WT) and *S. aureus* AD8 $\Delta ClfB$ with a diminution in adhesion frequency for the mutant. (B) Comparison of the adhesion force of *S. aureus* AD8 WT and *S. aureus* AD8 $\Delta ClfB$ (significantly different) (Fleury et al., 2017). (C) Maximum adhesion force and rupture distance distribution for the adhesion of *S. aureus* AD8 WT on low NMF skin samples and (D) on high NMF skin samples. (E) Topographic image obtain by contact imaging of a low NMF skin sample. (F) Topographic image obtain by contact imaging of a high NMF skin sample (Feuillie et al., Submitted).

1.4 Objectives

The main objective of this master thesis is to better understand the interactions between *S. aureus* and the human skin of AD patients, particularly in the case of low NMF skins where *S. aureus* has been shown to adhere more strongly. Our strategy is to use AFM to study the interactions both at the cellular and at the molecular levels.

Our first objective will be to investigate the role of several adhesins of *S. aureus* in its interaction with AD skins, i.e. ClfB, FnBPA and FnBPB (Fig. 1.15). We will use the AFM to perform single-cell force spectroscopy using different strains of *S. aureus* that carry or not the adhesins of interest, i.e. Wild Type (WT), $\Delta ClfB$, and $\Delta ClfB\Delta FnBPA\Delta FnBPB$. We will measure the percentage of adhesion, the force of adhesion and the length at which the interaction ruptures of the interaction occurs for each strain and on different samples of AD skin. As a direct follow-up to previous works performed in the laboratory, we will work with patient samples that present different NMF levels.

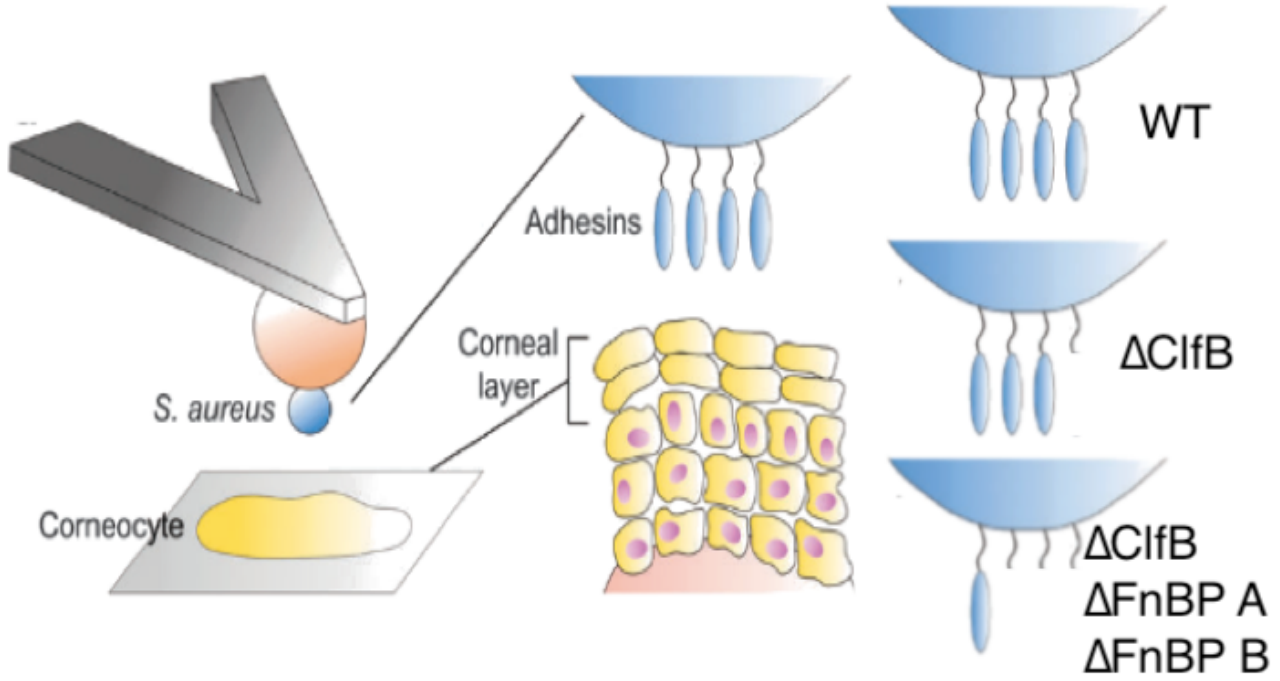

Figure 1.15: **Schematic protocol of the adhesion measurement between skin samples and different strains of *S. aureus* in this master thesis.** The adhesion will be measured between 3 strains of *S. aureus* (WT, $\Delta ClfB$, and $\Delta ClfB\Delta FnBPA\Delta FnBPB$) and the corneal layer of skin sample from patient suffering from Atopic dermatitis (AD).

Our second objective will be to study the role of corneodesmosin (CDSN) as a skin ligand for the adhesion of *S. aureus*. Abundant in the skin, CDSN has been recently identified has an *S. aureus* ligand (Geoghegan, 2018), but the molecular details of its interaction are poorly understood. We will first study the exposure of CDSN on low NMF skins, as well as locate it on corneocytes using single molecule force spectroscopy with a cantilever functionalized with an antibody directed against CDSN (Fig. 1.16 A). The single molecule force spectroscopy mode will give us maps of adhesion and topography as well as statistics of adhesion (force, rupture length).

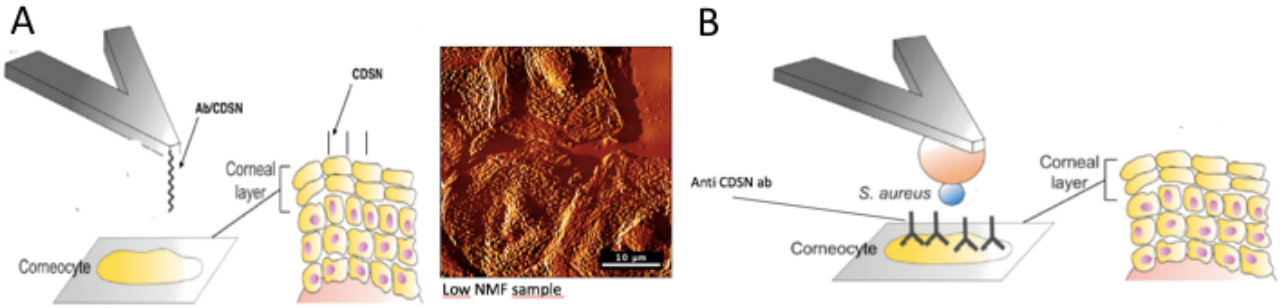

Figure 1.16: **Localizing and blocking CDSN ligands by AFM.** (A) Protocol for the localisation of the corneodesmosin (CDSN) on a skin sample by using a functionalized tip with an antibody anti-CDSN. (B) Protocol for the blocking of the interaction between *S. aureus* WT and AD skin sample with anti-CDSN antibodies.

We will then try to block the interaction of *S. aureus* with corneodesmosin by injecting an anti-CDSN antibody at different concentrations on the skin sample during the experiment (Fig 1.16 B). To measure the blocking, the adhesion between a single cell of WT *S. aureus* will be measured before and after injection of antibody, using the same cell on the cantilever. Through this method we will be able to assess whether the antibody really reduces the adhesion of *S. aureus* to the skin, and thus confirm or infirm that CDSN is involved as a ligand for *S. aureus* adhesion on skin, as well as identify which force of adhesion are involved in the CDSN interaction.

Chapter 2

Materials and methods

2.1 Bacterial cells and culture conditions

A clinical isolate strain of S.aureus, AD08 WT, from a patient suffering from Atopic dermatitis was stored in cryostocks at -80°C. Two other strains were also available ($\Delta ClfB$, $\Delta ClfB\Delta FnBPA\Delta FnBPB$). Mutant strains were designed following the method describe in Fleury et al. (2017). A first liquid culture was prepared from the cryostock ($15\mu l$ from cryostock in to 5ml of Trypticase soy broth (TSB)) overnight at 37°C under agitation at 180rpm within culture tube with dual-position caps that allow the air to come in. TSB agar plates were seeded from this overnight culture and used to prepare the overnight cultures used in our experiments. In the morning of the day of experimentation, cells were transferred in centrifugeable falcon tubes. They were centrifuged at 2000g for 3min at ambient temperature, and the supernatant was removed. To obtain exponential phase cultures, cells were re-suspended in TSB, and 100 μl of this cell suspension was added to 10ml of pre-warmed TSB at 37°C. The tube was then put at 37°C under agitation until an optical density at $\lambda = 600nm$ (OD_{600}) between 0.3 and 0.6 was reached. For stationary phase cultures, the cells were washed two times with Phosphate buffer saline (PBS) under centrifugations. Finally a 10x dilution was prepared and used for experiments. The cells of the exponential phase cultures were prepared following the same protocol when they had reached the appropriate OD_{600}.

2.2 Anti-CDSN antibodies

Full-length anti-CDSN antibody was purchased from AntibodyGenie (reference PACO0021120). The Fab fragment of anti-CDSN antibody was produced by our collaborators in Trinity College Dublin from this full-length antibody using a $Pierce^{TM} F(ab')2$ micro preparation kit (Fisher scientific).

2.3 Skin samples

The skin samples were provided by the lab of Pr. A. Irvine (Trinity college, Dublin). Skin samples were collected on the inner forearm of volunteer patients using circular adhesive strips ($3.8cm^2$, D-squame; Montaderm, Monaco, France), which were applied for 10 seconds on the skin, 8 times in a row (Formosa-Dague et al., 2016; Fleury et al., 2017). The 5 first were discarded, while the others are stored in a vial at -80°C. Skin samples were identified by patient numbers. A wide range of NMF skins were provided to us, and we focused in this study on the extreme cases, the # 1508 patient with low NMF skin (NMF = 0.14 mmol/g total protein) and the # 1493 patient with high NMF skin (NMF = 0.74 mmol/g total protein). NMF levels were measured by Pr. A. Irvine (Trinity college, Dublin) following a protocol previously described in Dapic et al. (2013).

2.4 Single Cells Force Spectroscopy (SCFS)

Before use, the cantilevers were washed with ethanol, dried with nitrogen and finally cleaned for 15 min under UV-Ozone-cleaner (Jelight Company Inc., Irvine California, USA) in order to avoid contamination. For SCFS experimentation we used tip-less cantilevers (NP-O10, Bruker) and we added a colloidal silica microsphere (6.1 μm of diameter, Bangs laboratories) by using UV-curable glue (NOA63, Northland Edmund Optics) and a Nanowizard III AFM (JPK instrument, Berlin, Germany). Before the experimentation, the cantilevers were immersed for 45 min in Tris Buffer Saline (TBS) (pH=8.5) containing 4mg/ml of dopamine hydrochloride (Sigma-Aldrich), then rinsed in TBS (3x) and finally mounted on the holder of the AFM, previously cleaned with soap, distilled water and ethanol and finally dried with nitrogen. Before any manipulation the cantilevers were calibrated in order to measure their sensitivity S $\sim$ 16 nm/V and their spring constant (k) $\sim$ 0.06 N/m by the thermal noise technique (Hutter and Bechhoefer, 1993).

The experimental set up consisted of an AFM petri dish in polystyrene, where a sample of skin was immobilized with double-sided tape, and a droplet of cells of *S. aureus* was deposited near the skin sample as shown in Figure 2.1. The dish was then filled with 2ml of PBS. A cell was immobilized on the silica bead by approaching an isolated cell and waiting 30 sec when the contact point was reached before retracting the tip. The presence of the cell was verified by optical microscopy and by measuring a force curve of the interaction between the surface of the dish and the tip before and after immobilization of the cell. Finally, if a cell was present, the interaction between the skin and the cell was measured. The standard experimental parameters were: room temperature, applied force of 0.25 nN, a constant approach-retraction speed of 1.0 $\mu m/s$ and a contact time of 100 ms. The size of the force maps was of 5 μm x 5 μm, 10 pixels x 10 pixels. For each cell, 4 maps were acquired.

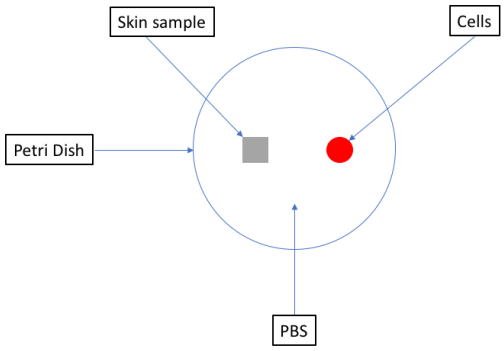

Figure 2.1: Set-up for SCFS experiments

2.5 Single molecule force spectroscopy (SMFS)

This method of spectroscopy was used to study CDSN on corneocytes. We functionalized a cantilever with an anti-CDSN antibody and tested 2 different methods of functionalization.

2.5.1 NHS-EDC

The first functionalization that we have used is the $NHS - EDC$ protocol. In this functionalization, we linked the protein to the tip through covalent liaison between $COOH$ groups on the tip and NH_2 groups in the antibody. Gold-coated cantilevers (OTR4-Gold, Olympus) were immersed in a bath of H_2O for 5 min, then an ethanol bath for 5 min, and finally they were dried with nitrogen. The cantilevers were then passed in the UV Ozone (Jelight Company Inc., Irvine California, USA) for 10 min. Afterwards the cantilevers were rinsed with ethanol and then dried with nitrogen.

Two 1 mM alkane thiols solutions were prepared, one with terminal $COOH$ groups (2.8 mg of 16-mercaptohexedecanoic acid in 10 ml of absolute ethanol) and the other with OH terminal groups (2.0 mg of 11-Mercator-1-undecanol in 10 ml of absolute ethanol). We then placed the cantilevers in a solution with 10% of $COOH$ and 90% of OH for $\sim$ 12 h (overnight), placed them in ethanol for 5 min and finally dried them with nitrogen.

The next step was to prepare a solution with 100 mg of N-(3-dimethylaminopropyl)-N-ethilcarbodiimide hydrochloride ($C_8H_{17}N$) (EDC) and 40 mg of N-hydroxysuccimide ($C_4H_5NO_3$) (NHS) in 4ml of ultrapure H_2O. The cantilevers were placed in this solution and incubated for 1 h at ambient temperature and were then rinsed in 3 successive baths of MilliQ water (Merck, Germany). The cantilevers were then placed on a parafilm surface with the tips in a drop of 100 μl of anti-CDSN antibody at a concentration of 0.1 mg/ml. They were incubated for 1h in the protein, rinced by 3 successive baths of PBS and subsequently used for experiment.

This first functionalization protocol did not lead to conclusive results (no interaction between the tip and the skin sample) and has therefore not been pursued further.

2.5.2 Gruber protocol

In this second chemistry, we linked the antibody to the tip via a linker, giving the protein more freedom. The cantilevers used in this protocol were the MSCT (Bruker, Germany), in silcon nitride.

First, the cantilevers were thoroughly cleaned in 3 successive bath of chloroform during 5 min each, followed by 15 min in the UV-Ozone cleaner (Jelight Company Inc., Irvine California, USA). They were then rinsed with ethanol and dried with nitrogen. To realize the amine functionalization, we then prepared an ethanolamine solution with 3.3 mg of ethanolamine in 6 ml of Dimethyl sulfoxide ($DMSO$) (Sigma-Aldrich). A teflon slide was put in the solution with molecular sieve of 0,3 nm (Milipore). The dish was put in a dessicator with a vacuum pump for $\sim$ 15 min to degas the molecular sieves and thus optimize the functionalization reaction. After that the cantilevers were placed on the teflon stick in the ethanolamine solution, and incubated overnight. The cantilevers were then immersed in 3 successive baths of $DMSO$ for 5 min each and then in 3 successive bath of absolute ethanol for 5 min each and finally dried with nitrogen.

To attach a linker on the tip to the NH_2 groups formed, we used Acetal-PEG-linkers purchased from the lab of Dr. Gruber (JKU, Linz, Austria) in sealed vials of 1 mg. We introduced 0.5 ml of chloroform and 30μl of triethylamine in the vial before putting the content in a cylindrical holder. The tips were immediately immersed and incubated for 2 hours at ambient temperature.

To complete the protein functionalization, the cantilever were first rinced in 3 successive baths of chloroform for 5 min each, then incubated in one bath of citric acid (50mg of citric acid in 50 ml of H_2O MilliQ (Merck, Germany)) for 10 min and finally rinced in 3 baths of H_2O miliQ for 5 min each. The cantilevers were then placed on a parafilm surface with the tip immerged in a drop of 100 μl of the anti-CDSN antibody at a concentration of 0.1 mg/ml. In the droplet, 2 μl of $NaCNBH_4$ (with 32 mg of $NaCNBH_3$ in 450 μl of H_2O MilliQ (Merck, Germany) and 50 μl of $NaOH$ 0.1 M) were added and it was incubated for 50 min. Finally to stop the reaction, 5 μl of ethanolamine (with 620 μl of ethanolamine in 10 ml of H_2O MilliQ (Merck, Germany) with a pH adjusted at 9.6) were added with an incubation of 10 min. The cantilevers were at last rinsed in 3 succesive baths of PBS and then stored in a solution of $PBS + NaN_3$ 0.01% in order to prevent oxidation.

2.6 CDSN localization using anti-CDSN tips

Multiparametric imaging of corneocytes with anti-CDSN tips was obtained by using the QI^{TM} mode available on the Nanowizard 3 AFM (JPK instruments, Germany). Images were obtained at 128 x 128 pixels with an applied force kept at 1 nN and a constant approach/retract speed of 40 $\mu m/s$. Force volumes of 32 x 32 curves were also acquired with 0.25 nN applied force and 1 $\mu m/s$ retract speed.

2.7 CDSN blocking

To block the CDSN, different concentration of the Fab fragment of anti-CDSN antibody were injected in the experimental set up during a SCFS experiment, without changing the cells. Successive force volumes of 10 x 10 pixels (4 per condition) were acquired on 5 μm areas to map the evolution of the interaction as a function of the concentration of Fab in the experimental volume. For this experience we have used a glass slide with an experimental area delimited by parafilm (Figure 2.2) to: 1) prevent any liquid spill in the objectives / microscope and 2) limit the volume of experimentation. The different concentration of Fab were: 0; 1.4; 2.6 ; 5 $\mu g/ml$ with an experimental volume of 250 μl in total (PBS + cell droplet + Fab).

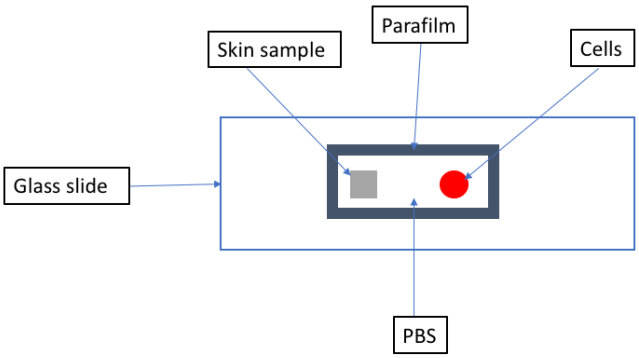

Figure 2.2: Set-up for the blocking experiments

2.8 Data processing and statistical analysis

Raw data were acquired in JPK files that can only be opened by the JPK data analysis software. With this software every curve of spectroscopy analysis was reviewed by the operator with a semi-automatic process taking into account the tip calibration (spring constant and the sensitivity), and the baseline level defined by the operator. For single cell force spectroscopy, we considered the rupture length of the last peak and the maximal force of adhesion. For single molecule force spectroscopy, we considered the rupture length and the adhesion of the last peak. The output file could be read by Excel (Microsoft Office) in order to extract the rupture length and the maximal adhesion. These data were then exported into Origin pro (OriginLab) for further analysis (Gaussian fits, means, etc).

Concerning the analysis of the images obtained in multiparametric imaging and force volume, using JPK data analysis we extracted the height image and the adhesion image. They were flattened and smoothed in order to avoid imaging artefacts due to topographic relief, and to exclude pixels with outlier values.

Chapter 3

Results and discussion

3.1 Adhesion of *Staphylococcus aureus* to low NMF skins

In order to decipher the role of the adhesins ClfB, FnBPA and FnBPB in the adhesion of *S. aureus* to human skin, we studied the adhesion of different strains of *S. aureus* AD08 expressing or not these surface proteins (WT, $\Delta ClfB$, $\Delta ClfB\Delta FnBPA\Delta FnBPB$). All strains and skin samples were kindled provided by our collaborators Dr. J. Geoghegan and Pr. A. Irvine from Trinity College Dublin. Unless stated otherwise, experiments have been conducted by SCFS in PBS buffer, in exponential growth phase on a skin sample with a low NMF level (patient # 1508, NMF = 0.14 mmol/g total protein) in agreement with earlier investigations (see section 1.3.2).

3.1.1 Adhesion of *S. aureus* AD08 WT

We measured the binding forces between *S. aureus* WT cells and low NMF skin using SCFS. Figure 3.1 presents the maximum adhesion force (A, D, G) and the rupture distance distribution (B, E, H), as well as characteristic force-distance curves (C, F, I) for 3 different WT cells interacting with low NMF skin, obtained at short contact time (100 ms) for 3 independent cells from independent cultures. Many force distance curves show multiple and well-defined adhesion peaks of up to 5000 pN in magnitude and 100 – 600 nm in rupture length. We measure a mean adhesion force of 1729 pN ± 1373 pN, and a mean rupture distance of 383 nm ± 156 nm (mean ± s.d., n= 632 adhesive curves from 3 different cells), with ∼ 59.5 % of interaction. Some cells present a single population of adhesion events, with 2276 pN ± 1029 pN (Fig. 3.1, Cell 2, mean ± s.d., n =191 adhesive curves). It is however frequent to observe 2 populations of adhesive forces (Cell 1 and 3, Fig. 3.1), with moderate forces ∼ 500 pN and high forces ∼ 1600 pN (mean ± s.d.: Cell 1: 1820 pN ± 1509 pN, n=260 adhesive curves; cell 3: 1027 pN ± 1176 pN, n = 180 adhesive curves). Some cells show a lower adhesion frequency (Cell 2, 47.9%) compared to others (Cell 1, 67.2%; Cell 3, 63.4%), further reflecting the heterogeneity of cellular population.

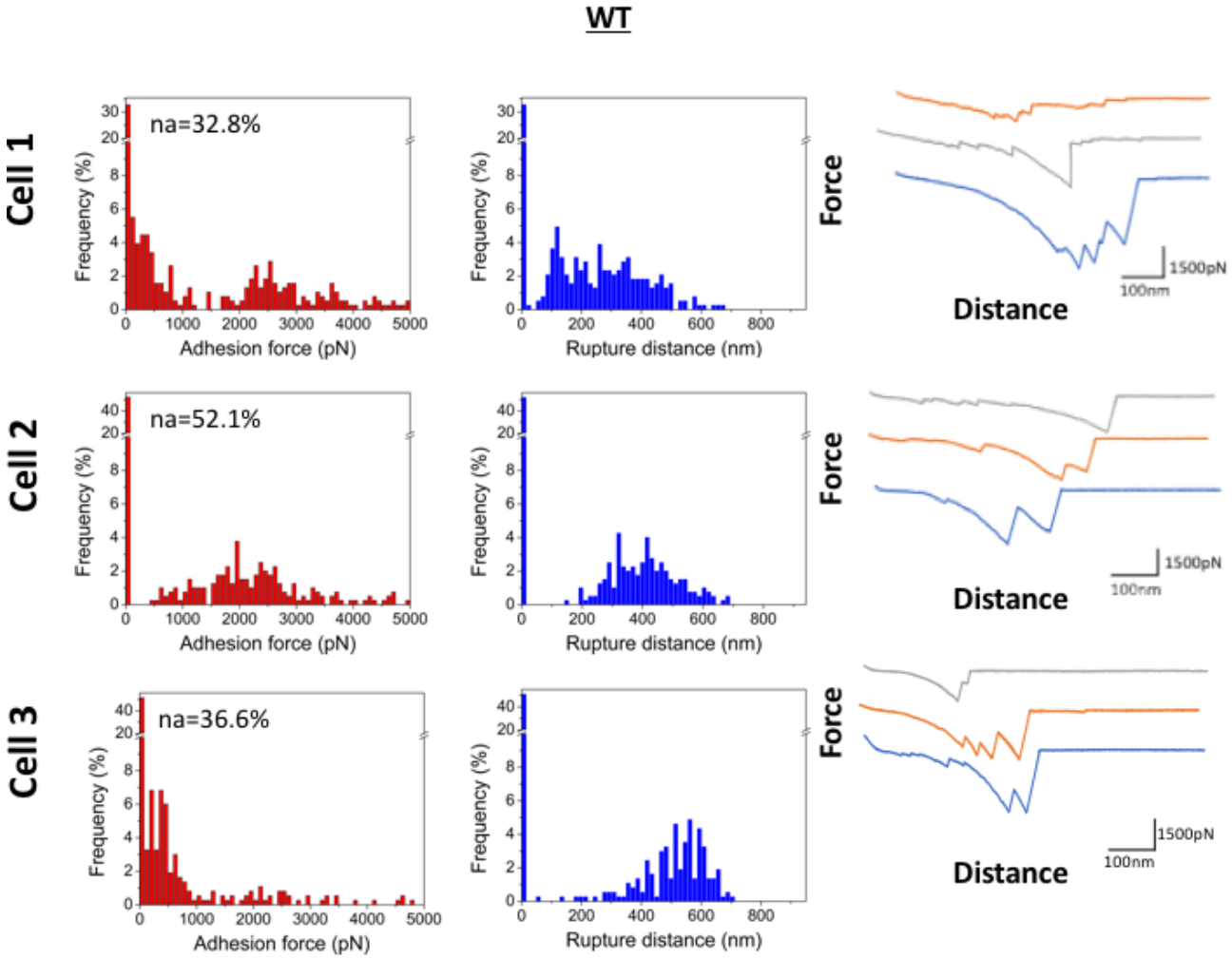

Figure 3.1: Maximum adhesion force (A, D, G), rupture distance distribution (B, E, H) and representative force-distance curves (C, F, I) for the adhesion of *S. aureus* AD08 *WT* (exponential phase of growth) on low NMF skin sample # 1508, for 3 independent cells (each cell = 400 force distance curves).

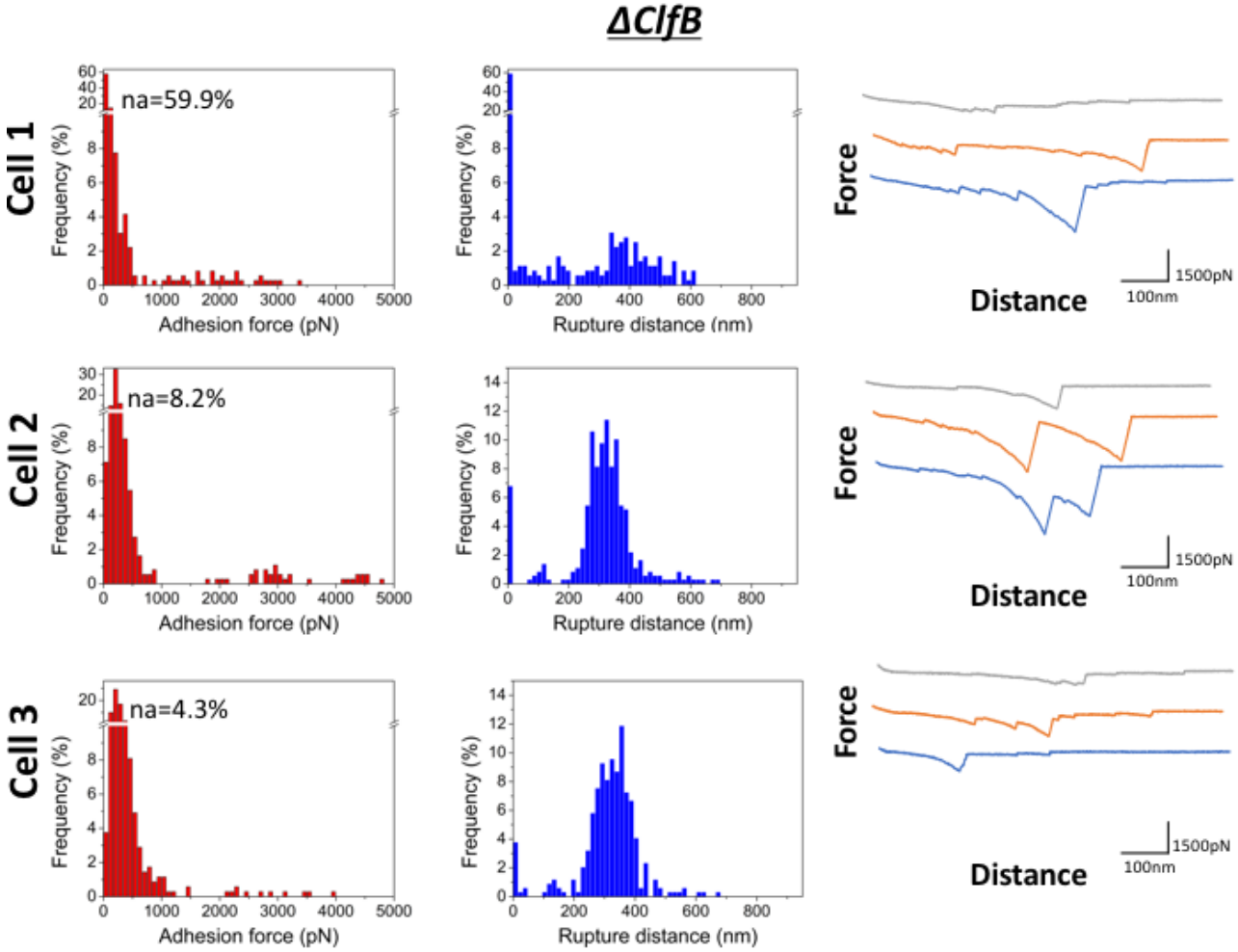

Figure 3.2: Maximum adhesion force (A, D, G) and rupture distance distribution (B, E, H) and characteristic force-distance curves (C, F, I) for the adhesion of *S. aureus* AD08 mutant $\Delta ClfB$ (exponential phase of growth) on low NMF skin sample # 1508, for 3 independent cells (each cell = 400 force distance curves).

3.1.2 Adhesion of the mutant strain *S. aureus* AD08 Δ *ClfB*

To understand the role of the ClfB adhesin, we then measured the adhesion of *S. aureus* AD08 $\Delta ClfB$, a mutant strain lacking the adhesin ClfB, to low NMF skin samples. Figure 3.2 presents the maximum adhesion force (A, D, G) and rupture distance distribution (B, E, H), as well as characteristic force-distance curves (C, F, I) for 3 different $\Delta ClfB$ cells interacting with low NMF skin, obtained at short contact time (100 ms) for 3 independent cells from independent cultures. As for the WT cells, many force distance curves show well-defined multiple adhesion peaks up to 4500 pN in magnitude, with most of the peaks below 1000 pN, and 100 – 600 nm in rupture length. We measure a mean adhesion force of 538 pN ± 843 pN (mean ± s.d., n = 827 adhesives curves from 3 different cells), which is about 3 times lower than for the WT strain. Concerning the rupture distance, the distribution is similar as for the WT strains with a mean of 328 nm ± 100 nm (mean ± s.d., n = 827 curves from 3 different cells), with ∼ 76.2% of interaction. The 3 cells present a single population of adhesion events, with 616 pN ± 801 pN (Fig. 3.2, Cell 1, n = 152 adhesives curves), 631 pN ± 1094 pN (Fig. 3.2, Cell 2, n = 344 adhesives curves), and 423 pN ± 508 pN (Fig. 3.2, Cell 3 n = 333 adhesives curves). We observe that the high forces present for the WT strain around 2000 - 2500 pN are less present to non-existent for the strain lacking ClfB, indicating that ClfB was responsible for these high forces. As for the WT strain, the adhesion frequency varies between cells with some adhering less than others (Fig. 3.2, Cell 1, 41% of adhesion; Cell 2, 91.8%; Cell 3, 95.7%), indicating a heterogeneity in the cellular population. The moderate forces are comparable to those observed in the WT strain, which indicates that adhesins other than ClfB are implicated in the process of adhesion. We therefore also studied the role of FnBP A and B.

3.1.3 Adhesion of the mutant strain *S. aureus* AD8 Δ*ClfB*Δ*FnBPA* Δ*FnBPB*

Following recent work (Krishna and Miller, 2012; Geoghegan, 2018), we have studied the role of FnBPA and B on the adhesion using a mutant strains of *S. aureus* AD08 $\Delta ClfB$ $\Delta FnBP$A $\Delta FnBP$B, strain lacking the adhesins ClfB, FnBPA and FnBPB, and hereafter referred to as triple mutant. Figure 3.3 presents the maximum adhesion force (A, D, G) and the rupture distance distribution (B, E, H), as well as representative force-distance curves (C, F, I) for 3 different triple mutant cells interacting with low NMF skin, obtained at short contact time (100 ms) for 3 independent cells from independent cultures. Compared to WT and $\Delta ClfB$ strains, the obtained force curves show fewer adhesion peaks, with a lower adhesion frequency and magnitude. We measure a mean adhesion frequency of ∼ 22 % and a mean adhesion force of 209 pN ± 287 pN (mean ± s.d., n = 314 curves from 3 different cells), which is about 4 times lower than for the WT strain. The 3 cells present a single population of adhesion events, with 324 pN ± 433 pN (Fig. 3.3, Cell 1, n = 80 adhesives curves), 161 pN ± 109 pN (Fig. 3.3, Cell 2, n = 181 adhesives curves) 208 pN ± 383 pN (Fig. 3.3, Cell 3, n = 51 adhesives curves). Concerning the rupture length, the distribution shows a rupture distance of 190 nm ± 212 nm (mean ± s.d., n=314 curves from 3 different cells), lower than for the WT and $\Delta ClfB$ strains, with some adhesion events still rupturing up to 600 nm. The cells present differences

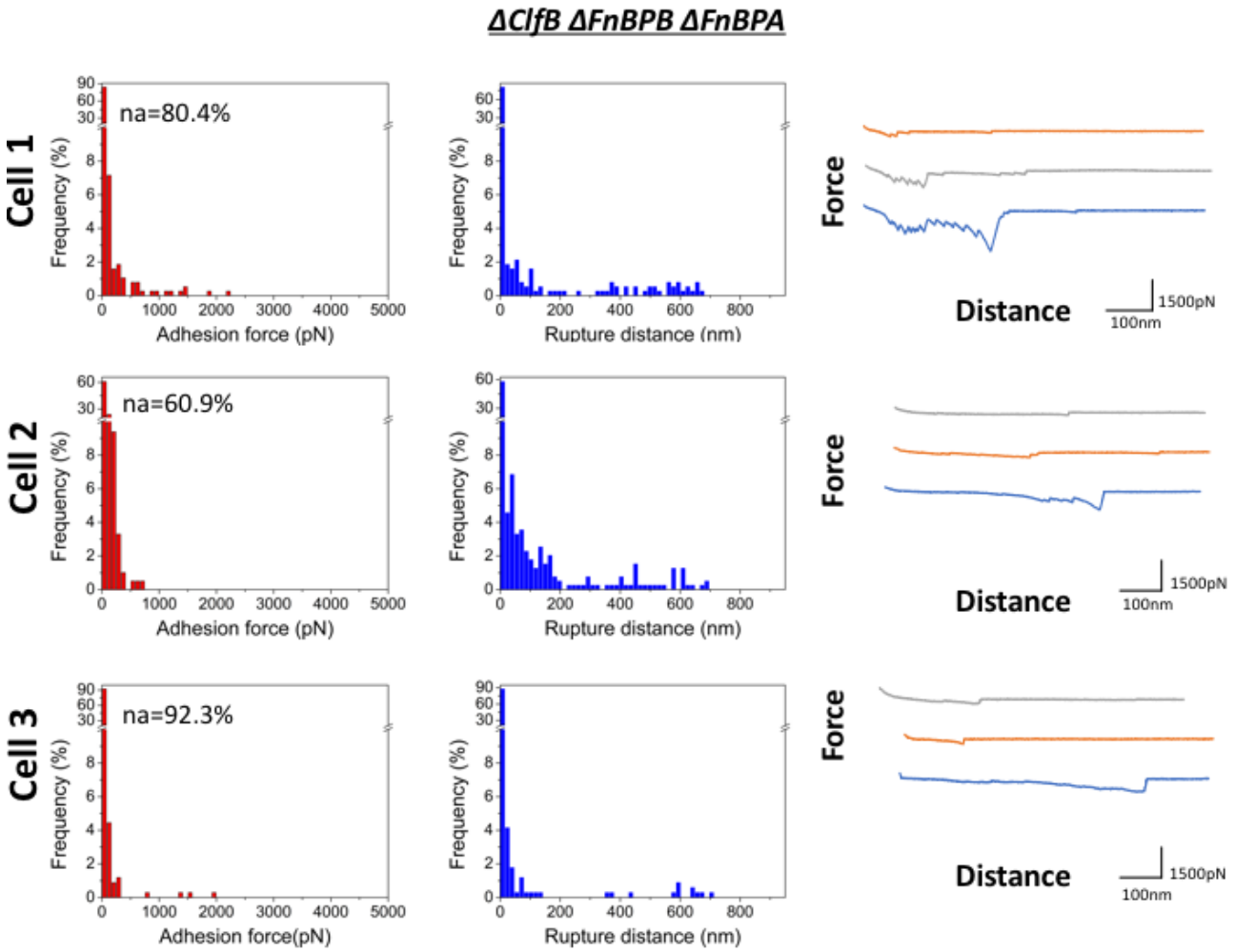

Figure 3.3: Maximum adhesion force (A, D, G) and rupture distance distribution (B, E, H) and characteristic force-distance curves (C, F, I) for the adhesion of *S. aureus* AD08 mutant $\Delta ClfB\Delta FnBPA\Delta FnBPB$ (exponential phase of growth) on low NMF skin sample 1508, for 3 independent cells (each cell = 400 force distance curves).

in the frequency of adhesion (3.3, Cell 1, 19.6%; Cell 2, 39.1%; Cell 3, 7.7%), representing a heterogeneous population. In summary, the above data show that both FnBPs and ClfB are involved in bacterial adhesion to AD skins and that their binding strength is moderate (500 pN) and high (1600 pN), respectively, thus suggesting two distinct binding mechanisms and/or ligands.

3.1.4 Effect of different growth phases on adhesion

Adhesins can be more or less expressed in function of the growth phase (O'Brien et al., 2002), which prompted us to study the effect of growth phase on the adhesion of *S. aureus* on skin in order to study in detail the role of the adhesins. We have thus compared the adhesion of the 3 different strains in stationary growth phase and exponential growth phase. These experiments were conducted by SCFS on low NMF skin (sample # 1508) in PBS buffer.

Figure 3.4 presents the maximum adhesion force for the 3 different strains tested in stationary (A, C, E) and exponential growth phase (B, D, F), as well as representative force-distance curves obtained at short contact time (100 ms). For each condition, 4 independent cells from independent cultures are presented. For the WT strain (Fig. 3.4 A, B), force curves between the two conditions do not present significant differences, though the rupture length distribution is narrower in stationary phase than in exponential phase. Indeed the standard deviation is smaller in the stationary phase than for the exponential phase: the rupture length for the WT strains is 340 ± 98 nm in stationary growth phase and 429 ± 528 nm in exponential growth phase (mean ± s.d., 4 cells). We observe a small decrease in adhesion frequency from stationary phase (69%) to exponential phase (56%). The mean force of adhesion is 711 pN ± 855 pN (mean ± s.d., n = 1128 adhesives curves for 4 different cells) for cells in stationary growth phase, compared to 1671 pN ± 1415 pN (mean ± s.d., n = 780 adhesives curves from 4 different cells) for cells in exponential growth phase. Moderate forces due to FnBPs are thus favoured in stationary phase and high forces, attributed to ClfB, are favoured in exponential phase. For the triple mutant (Fig. 3.4 C, D), the force curves for both growth phases are quite similar with little to no adhesion peaks. Contrary to WT cells, we observe for the triple mutant an increase of adhesion frequency between the stationary growth phase (13.9%) and the exponential growth phase (37.8%). The mean force of adhesion is increasing from 114 pN ± 61 pN (mean ± s.d., n = 336 adhesives curves from 4 different cells) for stationary growth phase cells to 424 pN ± 734 pN (mean ± s.d., n = 683 adhesives curves for 4 different cells) for exponential growth phase cells. This increase of forces between stationary and exponential growth phases is similar as the one observed for the WT strain. Finally, for the $\Delta ClfB$ mutant (Fig. 3.4 E, F), the force distance curves show for the two conditions well-defined peaks of adhesion. We observe a net increase of the percentage of adhesion between stationary growth phase (23.3%) and exponential growth phase (67.6%), that is ∼ two times higher than the increase observed for the triple mutant. The mean of the force of adhesion is again increasing from stationary to exponential growth phase, with a mean force of adhesion of 366 pN ± 547 pN (mean ± s.d., n = 748 adhesives curves for 4 different cells) for the stationary growth phase, and 515 pN ± 821 pN (mean ± s.d., n = 983 adhesives curves for 4 different cells) for the exponential growth phase.

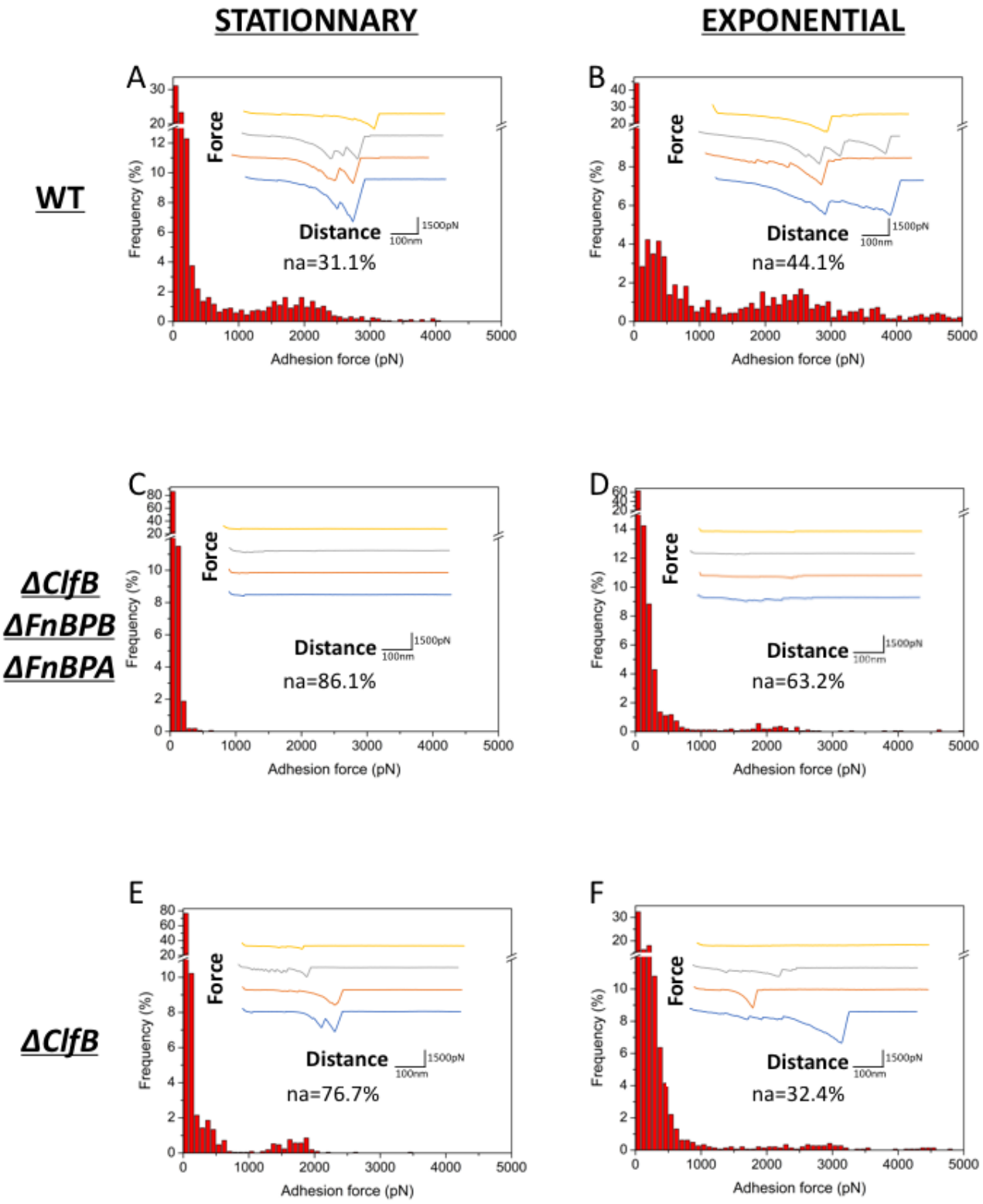

Figure 3.4: Maximum adhesion distribution and characteristic force-distance curve of the interaction between low NMF skin samples and different strains of *S. aureus* AD08: WT (A, B), triple mutant $\Delta ClfB\Delta FnBPA\Delta FnBPB$ (C, D), and $\Delta ClfB$ (E, F) in both stationary (A, C, E) and exponential growth phase (B, D, F). For each condition, we present the results from 4 independent cells, 4x400 force distance curves.

The exponential growth phase seems favour the expression and the availability of the FnBPA and B adhesins in the absence of ClfB. These results thus suggest that for studying ClfB it is better to work in exponential growth phase with the WT strains. For studying FnBPs, it is better to be in exponential phase with the $\Delta ClfB$ strains or in stationary phase with the WT strains.

3.2 Role of the corneodesmosin in the adhesion of *S. aureus* to AD skins

We then studied the role of corneodesmosin (CDSN) as a ligand for *S. aureus* in its adhesion to AD skins. For these experiments we used the SMFS mode to detect and locate CDSN on low NMF skins and the SCFS mode to prove its implication in the adhesion of *S. aureus*.

3.2.1 Localisation of corneodesmosin

To better understand the role of CDSN in the adhesion process, it was important to first locate it on the corneocyte. We thus performed experiments with AFM tips functionalized with anti-CDSN antibodies, following a functionalization protocol involving acetal linkers. Results are presented in Figures 3.5 and 3.6.

On figure 3.5, the adhesion force distribution for the interaction of anti-CDSN tips with low NMF skin shows an average percentage of adhesion of 8% (mean adhesion frequency for 4 tips). The results obtained with 4 independent AFM tips present the same distribution pattern with a majority of low forces and a mean adhesion force of 80.7 pN ± 78.1 pN (mean ± s.d., n=328 curves for 4 different tips), consistent with antibody-ligand interactions (Chen et al., 2011; Müller et al., 2009). In contrast, the interaction with high NMF skin presents an average percentage of adhesion of 2.5% (mean adhesion frequency for 4 tips), which is 3 times lower than for low NMF skin. We can observe a diminution in the frequency of low forces in comparison with the forces observed for the low NMF skin. The mean of adhesion is 103.1 pN ± 93.3 pN (mean ± s.d., n=101 curves for 4 different cells). These results show that CDSN is more abundant on low NMF skin than on high NMF skin, thus suggesting it is a ligand for *S. aureus* adhesins.

Figure 3.6 shows in A and B height and adhesion images obtained by multiparametric imaging, or QI^{TM}, on low NMF skin (sample # 1508, NMF = 0.14 mmol/g total protein) using anti-CDSN tips. The lighter spots on the adhesion pictures correspond to adhesion events, indicating the presence of CDSN. Comparing with Fig. 3.6 C and D, obtained on high NMF skin (sample # 1493, NMF = 0.74 mmol/g total protein), we observe that there are fewer events of adhesion on high NMF skin than on low NMF skin. This confirms that CDSN is more abundant on low NMF skin. From our results it is however not possible to say if CDSN concentrates on the tip of the vilous protrusions or not.

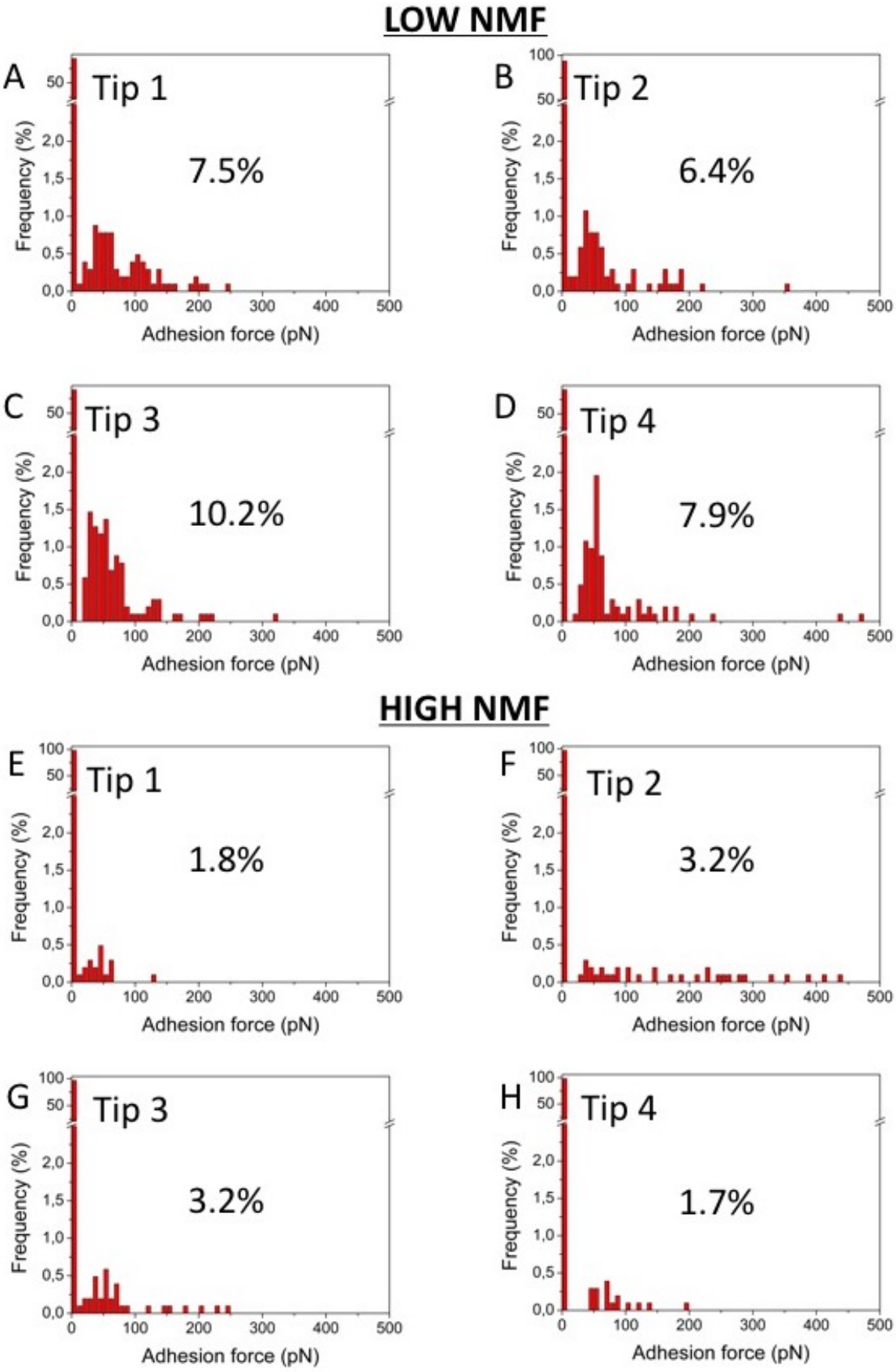

Figure 3.5: Maximum adhesion force distribution and percentage of interaction between an AFM tip functionalized with an anti-CDSN antibody and low (sample # 1508) (A, B, C, D) or high (sample # 1493) (E, F, G, H) NMF skin samples. Each histogram presents 1024 force distance curves from 1 independent tip obtained in SMFS mode with AFM. Each tip was used on both low NMF and high NMF.

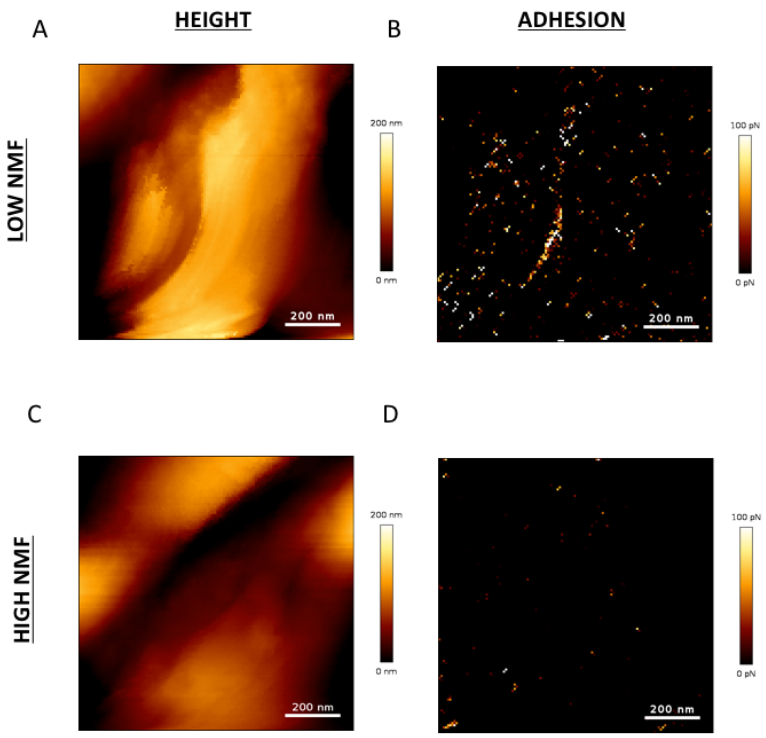

Figure 3.6: Image of height (A, C) and adhesion (B, D) of the interaction between an AFM tip functionalized with an anti-CDSN antibody and low (sample # 1508) (A, B) and high (sample # 1493) (D, E) NMF skin samples. Images were obtained by multiparametric imaging.

3.2.2 Blocking of corneodesmosin

To further validate that CDSN is effectively playing a role in the adhesion of *S. aureus* on AD skin, we tried to block it on the skin by injecting different concentrations of Fab fragments of the anti-CDSN antibody. This antibody fragment was provided by Dr. J. Geoghegan (Trinity College, Dublin) and is designed to target a specific loop of the CDSN that should be exposed on the surface of the skin. Having identified low NMF skins as preferential surfaces for the study of CDSN, we performed this experiments on low NMF skin only. The blocking experiments were realised by SCFS, with *S. aureus* AD08 *WT* cells in stationary phase with injection of different concentrations of Fab fragments of anti CDSN antibody in the experimental volume. The stationary phase was chosen to simultaneously test the interaction between both FnBP and ClfB and CDSN. Indeed, the comparison of the effect of the two growth phases has shown that both ClfB and FnBPs are present in stationary phase for the *WT* strain and that FnBP interactions are favored. Results are presented in Fig. 3.7.

When we increase the Fab concentration, we observe for 5 cells a decrease of the normalized percentage of interaction from 100% of interaction to 80 - 55% of interaction (Fig. 3.7 A). We do observe some variability and for 2 cells, no decrease in term of percentage of interaction was recorded. Figure 3.7 B shows the evolution of the distribution of maximum adhesion force as a function of the increasing concentration of Fab for the red cell (Fig. 3.7 A). There is a net decrease of the percentage of adhesion, evolving from 73.1% to 54.4% at 0 $\mu g/ml$ and 2.6 $\mu g/ml$ of Fab, respectively, followed by a plateau between 2.6 $\mu g/ml$ and 5 $\mu g/ml$. Some of the cells, therefore show partial blocking of the interaction. *S. aureus* / low NMF skin.

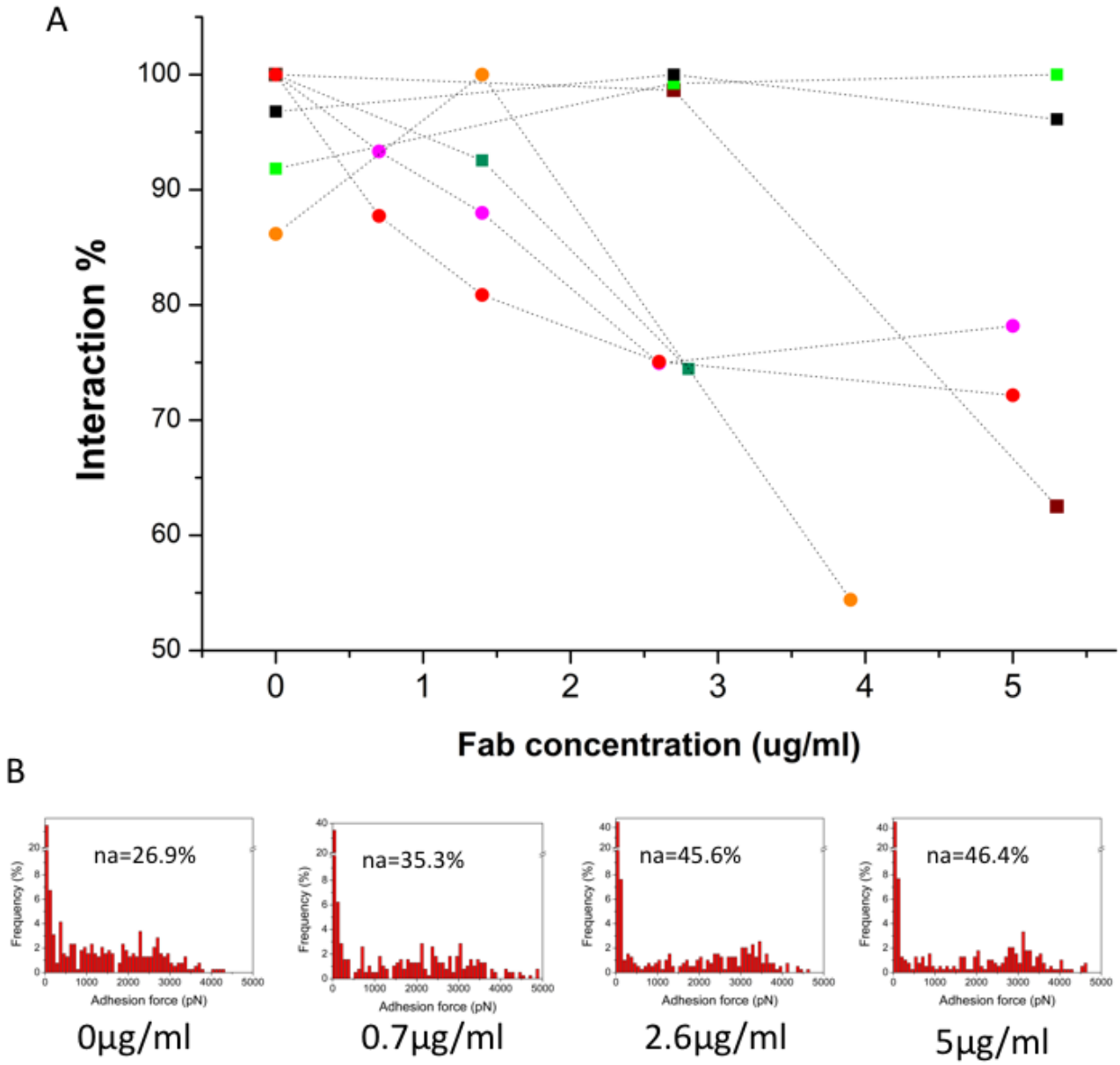

Figure 3.7: Evolution of the normalized percentage of interaction between cells of *S. aureus* AD08 *WT* in stationary phase and low NMF skin samples 1508, as a function of the anti-CDSN Fab fragment concentration injected in the experimental volume (1color = 1cell, dashed lines are guides for the eyes) (A). Maximum adhesion force distribution of this interaction at different Fab concentrations (B).

Table 3.1: Number of high and low forces curves for a concentration of $0\mu g/ml$ and $5\mu g/ml$ of Fab fragment of the anti-CDSN antibody

Cells	**Concentration** ($\mu g/ml$)	**Number of Low forces events** ($\leq 913pN$)	**Number of High forces events** ($> 913pN$)
Red cell	0	103	195
	5	67	148
Pink cell	0	106	257
	5	93	202
Brown cell	0	136	61
	5	85	43

We tried to quantify which adhesin (FnBP or ClfB) was most affected by the blocking. From Fig. 3.7 B low and high forces seem to be reduced in a similar proportion, suggesting that CDSN might be a ligand for both FnBPs and ClfB on low NMF skins. We have calculated the number of low and high forces adhesion events for the minimum and maximum concentration of Fab fragment for the cells presented in red, pink and brown on figure 3.7 and the results are presented in Table: 3.1. The limit between low and high force adhesion has been determined as the mean plus standard deviation of the adhesion of the $\Delta ClfB$ mutant in stationary growth phase (366 pN + 547 pN = 913 pN). Forces are considered as low and attributed to FnBPs if they are below or equal to 913 pN, and are considered as high and attributed to ClfB if they are higher than 913 pN.

We can see a diminution of the number of curves from the low Fab concentration to the high concentration for the 3 cells for both low and high forces adhesion events. For the red cell low forces diminish by 35% while high forces diminish by 24%; for the pink cell, low forces diminish by 12% while high forces events decrease by 21%; for the brown cell low forces diminish by 38% while high forces events decrease by 30%.

The mean of the diminishing percentage is 28% for the low forces and 25% for the high forces. The two percentages are close, which indicates that CDSN interact with both ClfB and FnBP.

Chapter 4

Conclusions

The bacterial pathogen *S. aureus* plays an important role in Atopic dermatitis (AD), a chronic disorder that mostly affects children. Colonization of the skin of AD patients by *S. aureus* exacerbates the disease, but the molecular determinants of the bacterial-skin adhesive interactions are still poorly understood (Fleury et al., 2017; Vitry et al., 2017). Low NMF levels in the *stratum corneum* has been shown to be associated with more severe AD symptoms (Palmer et al., 2006), but whether this is directly related to *S. aureus* adhesion is unclear. In this work we used AFM to examine the mechanism of adhesion of *S. aureus* to AD skins with the following questions in mind: i) what are the bacterial adhesins involved in *S. aureus* - skin adhesion, and ii) is the skin protein CDSN a major ligand for *S. aureus* adhesins?

4.1 Both ClfB and FnBPs play a role in *S. aureus* - skin adhesion

By studying mutant strains of *S. aureus* with deleted adhesins by SCFS, we found that both ClfB and $FnBPs$ play a role in mediating *S. aureus* adhesion to low NMF skins. Comparing the adhesion force distributions between *S. aureus* AD08 WT and $\Delta ClfB$ strains in exponential phase confirmed that ClfB is a major adhesin implicated in the process of adhesion, in agreement with the literature (Vitry et al., 2017; Mulcahy et al., 2012). Moreover, the variation of the distribution of the adhesion force showed that the forces between 1000 and 3000 pN are the most affected by the removal of ClfB. The ligand of ClfB on human skin has been identified as loricrin (Mulcahy et al., 2012). Furthermore, the interaction between ClfB and loricrin has been previously characterized by SCFS and SMFS (Vitry et al., 2017), and it involves the mechanism of Dock Lock and Latch with an average force of adhesion of 1500 pN. The high forces observed between *S. aureus* AD08 WT and low NMF skin are therefore consistent with the ClfB – loricrin interaction. The mean adhesion force measured for AD08 WT in exponential phase and low NMF skin is 1700 pN, very close to the force reported for the ClfB / loricrin interaction. We can therefore assume that the interaction between *S. aureus* AD08 WT in exponential phase and the skin is dominated by this interaction. We observe a mean rupture length of 400 nm. In the case of the interaction of *S. aureus* AD08 WT with model surfaces of loricrin, measured by Vitry et al. (2017), the rupture length observed are of 140 nm. Considering that 1 amino

acid (aa) accounts for 0.36nm (Oesterhelt, 2000), the length of unfolded ClfB can be calculated: with 860 aa, full length ClfB is $\sim$ 310nm. The protein in the unfolded state is about 25 nm, so the full length measured by AFM should be about 285 nm. Though ClfB was not unfolded in model surfaces experiments (Vitry et al., 2017), the observed length in our experiments is higher than the length of ClfB only. One explanation could be that the loricrin is also unfolded during the retraction phase. The loricrin protein is a 312 aa protein, indicating an unfolded size of $\sim$ 112 nm. If the two proteins are unfolded, a length of 397 nm should be observed, which is close to the rupture length that we obtained (380 nm). Our results in comparison with the one of Vitry et al. (2017) show that it is possible to see more details and better understand adhesion mechanisms in biological context than on model surfaces.

Comparing the adhesion results between *S. aureus* AD08 $\Delta ClfB$ and triple mutant (Δ *ClfB* Δ *FnBPA* Δ *FnBPB*) strains confirmed the involvement of FnBP A and B in the process of adhesion of *S. aureus* to human skin, in agreement with literature (Geoghegan et al., 2013). From 28% in the case of *S. aureus* AD08 Δ ClfB, the percentage of non-adhesion climbs to 78% in the case of the triple mutant lacking ClfB, FnBP A and B, thus highlighting their role as preferential actors of adhesion. The residual adhesion ($\sim$ 22%) indicates that other adhesins are interacting with the skin, but to a lesser extent than ClfB and FnBP A and B. Forces measured for *S. aureus* AD08 Δ ClfB are $\sim$ 538 pN, and can therefore be attributed to FnBP A and B, as well as the lower forces (below 1000 pN) observed for *S. aureus* AD08 WT. If we compare the percentage of adhesion for the Δ ClfB and the WT strain, there is an augmentation for the mutant strain: 59.5% for the WT strain in exponential growth phase and 67.6% of adhesion for the Δ ClfB strain in exponential growth phase. This result means that even if we have deleted one of the major adhesins that is ClfB, the percentage of adhesion in not descending in percentage. This observation could be consistent with the fact that ClfB in WT exponential growth phase is shielding FnBP, preventing it to interact with the skin. If we look at the size of ClfB and FnBP, ClfB is made of 860 aa and FnBP 486 aa, so ClfB could be rising above FnBP on the surface of *S. aureus*, which would make ClfB more accessible for its ligands.

As said above, the unfolded size of FnBP is 175 nm, which is lower than the rupture length observed for the adhesion of the Δ ClfB mutant $\sim$ 330 nm: this would indicate that not only FnBP is unfolding, and brings up the question of identifying the ligand of FnBP on human skin.

4.2 CDSN is a ligand for *S. aureus* on AD skins

Following work by our collaborators from Trinity College, Dublin, we have investigated CDSN as a ligand on the skin for *S. aureus* and its adhesins. The first step to identify the ligand was to determine the best conditions in which we should study the interaction to have access to both FnBPs and ClfB. We have first determined the optimal growth phase for the bacteria by comparing the stationary and exponential growth phase for each strain. This has allowed us to highlight differences in adhesive behaviour in function of the strain. For the WT strain, there is a shift in terms of adhesion forces between stationary and exponential growth phase. The mean adhesion force passed from 710 pN for stationary growth phase cells to 1700 pN for

exponential growth phase cells. Lower forces are more abundant in stationary growth phase than in exponential growth phase. Indeed, we have established that ClfB is responsible for the higher forces, and O'Brien et al. (2002) has reported that ClfB is more expressed on the surface of *S. aureus* during the exponential growth phase. Stationary phase seems then to be the optimal growth phase to study FnBP, knowing that FnBP is responsible for the lower forces that are more visible during this growth phase, while still observing the impact of ClfB. To study the role of FnBPs alone, one other strain could have been used, the Δ ClfB strain in exponential growth phase. Being a clinical isolate, the AD8 WT strain is however the most relevant strain.

It was then important to confirm whether CDSN is expressed on our skin samples, and on which NMF level we should test our hypothesis. To do so, we have tried to locate CDSN on both a low NMF skin sample (# 1508, NMF=0.14 mmol/g total protein) and on a high NMF skin sample (# 1493, NMF=0.74 mmol/g total protein) using tips functionalized with anti-CDSN antibody. The results of the localisation experiment have shown that the low NMF skin present a significantly higher level of events of adhesion (8% low NMF, 2.5% high NMF) showing that CDSN is more expressed on this skin. We can compare our results to a similar study: Rankl et al. (2010) have also tried to locate CDSN, though on healthy skin, using AFM and antibody functionalized tips. What is similar in both experiments is the percentage of adhesion, which is between 5-10% for them and 8% for us and the average adhesion forces, which are around 80 pN for both experiments. This confirms that the interaction measured in our experiment is indeed a CDSN-antibody interaction. Multiparametric imaging also showed a higher proportion of adhesive events on low NMF skin compared to the high NMF skin, confirming the higher exposition of CDSN on low NMF skin. Overall these observations show that CDSN is more abundant on low NMF skins, compared to high NMF skins, thus suggesting it could be an important ligand for *S. aureus* adhesins. One way to understand this phenomenon is to go back to the source of the NMF, which is filaggrin. Low NMF skins are due to a reduced filaggrin availability (Fowler, 2012). This lack of filaggrin is also expressed on the skin by more abundant protrusions on the skin, which has been confirmed by AFM imaging (Formosa-Dague et al., 2016; Fleury et al., 2017), due to dehydration. These protrusions bring CDSN to the surface of low NMF skin, while it would not be "raised" or "exposed" otherwise because CDSN is localized in corneodesmosomes that hold corneocytes together (Kitajima, 2015). Riethmuller et al. (2015) have described this phenomenon by immunolabelling: WT patients with no loss of function mutations of the filaggrin gene (FLG) presented exposed CDSN on the edge of the corneocytes only, while patients with FLG loss of function mutations presented CDSN over the whole surface of the corneocytes, and in most cases but not all on the tip of the protrusions. In their study of healthy skin, Rankl et al. (2010) have managed to locate CDSN on skin on top of protrusions, which in our case cannot be said, as we do not observe any preferential localisation for CDSN on low NMF skin images. Concerning multiparametric imaging, we have to be careful about our results. Even though most events of adhesion are consistent with an interaction between the CDSN and the antibody, some events might be attributed to imaging artefacts / topographic effect due to the height of the protrusion, thus leading to "side" effects delimiting the edge of the villus protrusion.

To be able to assess whether CDSN is a ligand of FnBP, ClfB, or both, we have blocked the interaction between *S. aureus* in stationary phase and low NMF skin where CDSN is most abundant by injecting a fragment of anti-CDSN antibody, Fab. The results obtained have shown a diminution in adhesion frequency for some cells resulting from the injection of the Fab fragment of the anti-CDSN antibody, strengthening with higher concentrations. Since the blocking works, it allows us to confirm that CDSN is a ligand for *S. aureus*.

The fact that some cells do not show a significant decrease could be explained by the variability due to the localisation of the measurement. Indeed, the localisation results have shown that we don't locate CDSN everywhere on the skin. The distribution of forces of the different cells and their percentage of respectively high and low forces bring us to consider that CDSN is a ligand of FnBP but also of ClfB, as both populations of adhesion events show a similar decrease in frequency. Knowing CDSN is a ligand for FnBPs, we can propose a hypothesis for the rupture length observed with the Δ ClfB mutant: with 328nm it is bigger than the unfolded length of FnBP alone (175nm), which indicates the unfolding of an extra protein. The length of the CDSN is 529 aa, which corresponds to 190 nm. If again we suppose that the two proteins are totally unfolding during the retract phase, the rupture length that we should observe for FnBP + CDSN is 365 nm, which is close to the rupture length observed (328+/-100nm). This reinforces the hypothesis that CDSN is a ligand for FnBP.

To gain further insight into this CDSN / FnBP interaction, additional experiments should be envisioned. For example, SCFS could be performed with both WT and Δ ClfB cells on a CDSN-coated surface. Moreover, it will be worth using a functionalized tip with CDSN to probe the CDSN / FnBP and CDSN / ClfB interactions directly on a *S. aureus* cell in exponential growth phase, or on a WT cell in exponential growth phase, respectively. These techniques have been used by Vitry et al. (2017) in order to confirm that loricrin was the ligand of ClfB on the skin. Finally, a new mutant strain, lacking FnBPA and B but expressing ClfB, could be studied, in order to complete the set of mutant and fully decipher the own role of ClfB, FnBPA and B.

All together, our results shed new light into the molecular determinants of *S. aureus*-AD skin interactions: i) ClfB and FnBPs are the main adhesins involved; ii) the binding strengths of ClfB and FnBPs are high and moderate, respectively, suggesting that two different ligands and / or mechanisms are involved; iii) CDSN seems to be an important ligand for FnBPs, but also for ClfB.

Our study opens up new possibilities for the development of anti-adhesive therapies to prevent *S. aureus* from attaching to human skins. This kind of therapy consists in blocking the ligands on the skin to make them inaccessible for *S. aureus*, or of targeting the adhesins themselves. A technique to target the ligand would consist in covering the skin with identified adhesin partners, blocking its interaction with bacterial cells. This has the major advantages of not leading the bacteria to develop any resistance because it doesn't affect the bacteria viability, and thus doesn't create a selective pressure who would make bacteria develop resistance (Krachler and Orth, 2013). However, the major difficulty consist in the fact that there are multiple adhesins interacting with several ligands on the skin. Therefore blocking just one of the ligands or the adhesins will not be sufficient to avoid the adhesion of the bacteria. In the

case of *S. aureus* several adhesins have already been putt forward as major actors of adhesion on skin. In order to reach the avidity level to compete with *S. aureus*, the anti-adhesive solution should include several adhesins. Some solutions have already been proposed such as using polymers where different adhesins are tethered (Krachler and Orth, 2013). When this polymer is in contact with the skin, it enters in competition with *S. aureus* and block the different ligand on the skin (Krachler and Orth, 2013). Antibodies capable of specifically blocking adhesins of *S. aureus* have also been discovered and tested, such as monoclonal antibodies targeting the *S. aureus* collagen-binding protein Cna (Herman-Bausier et al., 2016).

Bibliography

Albrecht, T. R., Grütter, P., Horne, D., Rugar, D., Jan. 1991. Frequency modulation detection using high- Q cantilevers for enhanced force microscope sensitivity. Journal of Applied Physics 69 (2), 668–673.
URL http://aip.scitation.org/doi/10.1063/1.347347

Beaussart, A., El-Kirat-Chatel, S., Sullan, R. M. A., Alsteens, D., Herman, P., Derclaye, S., Dufrêne, Y. F., Apr. 2014. Quantifying the forces guiding microbial cell adhesion using single-cell force spectroscopy. Nature Protocols 9 (5), 1049–1055.
URL http://www.nature.com/doifinder/10.1038/nprot.2014.066

Bieber, T., Apr. 2008. Atopic Dermatitis. New England Journal of Medicine 358 (14), 1483–1494.
URL http://www.nejm.org/doi/abs/10.1056/NEJMra074081

Binnig, G., Quate, C. F., Gerber, C., Mar. 1986. Atomic Force Microscope. Physical Review Letters 56 (9), 930–933.
URL https://link.aps.org/doi/10.1103/PhysRevLett.56.930

Binnig, G., Rohrer, H., Gerber, C., Weibel, E., Jul. 1982. Surface Studies by Scanning Tunneling Microscopy. Physical Review Letters 49 (1), 57–61.
URL https://link.aps.org/doi/10.1103/PhysRevLett.49.57

Chen, Y., Zeng, G., Chen, S. S., Feng, Q., Chen, Z. W., Apr. 2011. AFM force measurements of the gp120–sCD4 and gp120 or CD4 antigen–antibody interactions. Biochemical and Biophysical Research Communications 407 (2), 301–306.
URL http://linkinghub.elsevier.com/retrieve/pii/S0006291X11003780

Cho, S.-H., Strickland, I., Boguniewicz, M., Leung, D. Y., Aug. 2001. Fibronectin and fibrinogen contribute to the enhanced binding of *Staphylococcus aureus* to atopic skin. Journal of Allergy and Clinical Immunology 108 (2), 269–274.
URL http://linkinghub.elsevier.com/retrieve/pii/S0091674901233454

Dapic, I., Jakasa, I., Yau, N. L. H., Kezic, S., Kammeyer, A., 2013. Evaluation of an hplc method for the determination of natural moisturizing factors in the human *Stratum Corneum*. Analytical Letters 46 (14), 2133–2144.

Dufrêne, Y. F., Jun. 2015. Sticky microbes: forces in microbial cell adhesion. Trends in Microbiology 23 (6), 376–382.
URL http://linkinghub.elsevier.com/retrieve/pii/S0966842X15000256

Dufrêne, Y. F., Ando, T., Garcia, R., Alsteens, D., Martinez-Martin, D., Engel, A., Gerber, C., Müller, D. J., Apr. 2017. Imaging modes of atomic force microscopy for application in molecular and cell biology. Nature Nanotechnology 12 (4), 295–307.
URL http://www.nature.com/doifinder/10.1038/nnano.2017.45

Dufrêne, Y. F., Martínez-Martín, D., Medalsy, I., Alsteens, D., Müller, D. J., Aug. 2013. Multiparametric imaging of biological systems by force-distance curve–based AFM. Nature Methods 10 (9), 847–854.
URL http://www.nature.com/doifinder/10.1038/nmeth.2602

Ebner, A., Hinterdorfer, P., Gruber, H. J., Oct. 2007. Comparison of different aminofunctionalization strategies for attachment of single antibodies to AFM cantilevers. Ultramicroscopy 107 (10-11), 922–927.
URL http://linkinghub.elsevier.com/retrieve/pii/S0304399107001040

Feuillie, C., Vitry, P., McAleer, M. A., Kezic, S., Irvine, A. D., Geoghegan, J. A., Dufrêne, Y. F., Submitted. Adhesion of *Staphylococcus aureus* to corneocytes from atopic dematitis patients is controlled by natural moisturizing factor levels.

Fleury, O. M., McAleer, M. A., Feuillie, C., Formosa-Dague, C., Sansevere, E., Bennett, D. E., Towell, A. M., McLean, W. H. I., Kezic, S., Robinson, D. A., Fallon, P. G., Foster, T. J., Dufrêne, Y. F., Irvine, A. D., Geoghegan, J. A., Jun. 2017. Clumping Factor B Promotes Adherence of *Staphylococcus aureus* to Corneocytes in Atopic Dermatitis. Infection and Immunity 85 (6), e00994–16.
URL http://iai.asm.org/lookup/doi/10.1128/IAI.00994-16

Formosa-Dague, C., Fu, Z.-H., Feuillie, C., Derclaye, S., Foster, T. J., Geoghegan, J. A., Dufrêne, Y. F., 2016. Forces between *Staphylococcus aureus* and human skin. Nanoscale Horiz. 1 (4), 298–303.
URL http://xlink.rsc.org/?DOI=C6NH00057F

Foster, T. J., Cameron, B. J., Peacock, S. J., Berendt, A. R., Dec. 1999. Bacterial fibronectin-binding proteins and endothelial cell surface fibronectin mediate adherence of *Staphylococcus aureus* to resting human endothelial cells. Microbiology 145 (12), 3477–3486.
URL http://mic.microbiologyresearch.org/content/journal/micro/10.1099/00221287-145-12-3477

Foster, T. J., Geoghegan, J. A., Ganesh, V. K., Höök, M., Dec. 2013. Adhesion, invasion and evasion: the many functions of the surface proteins of *Staphylococcus aureus*. Nature Reviews Microbiology 12 (1), 49–62.
URL http://www.nature.com/doifinder/10.1038/nrmicro3161

Fowler, J., 2012. Understanding the role of natural moisturizing factor in skin hydration. Pract. Dermatol., July, 36–40.

Gaboriaud, F., Dufrêne, Y. F., Jan. 2007. Atomic force microscopy of microbial cells: Application to nanomechanical properties, surface forces and molecular recognition forces. Colloids and Surfaces B: Biointerfaces 54 (1), 10–19.
URL http://linkinghub.elsevier.com/retrieve/pii/S0927776506002931

Geoghegan, J. A., Jan. 2018. Personal communication, skin project.

Geoghegan, J. A., Monk, I. R., O'Gara, J. P., Foster, T. J., Jun. 2013. Subdomains N2n3 of Fibronectin Binding Protein A Mediate *Staphylococcus aureus* Biofilm Formation and Adherence to Fibrinogen Using Distinct Mechanisms. Journal of Bacteriology 195 (11), 2675–2683.
URL http://jb.asm.org/cgi/doi/10.1128/JB.02128-12

Greenwood, D., O'Grady, F., Apr. 1972. Scanning Electron Microscopy of *Staphylococcus aureus* Exposed to Some Common Anti-staphylococcal Agents. Journal of General Microbiology 70 (2), 263–270.
URL http://mic.microbiologyresearch.org/content/journal/micro/10.1099/00221287-70-2-263

Grice, E. A., Segre, J. A., Apr. 2011. The skin microbiome. Nature Reviews Microbiology 9 (4), 244–253.
URL http://www.nature.com/articles/nrmicro2537

Herman-Bausier, P., Valotteau, C., Pietrocola, G., Rindi, S., Alsteens, D., Foster, T. J., Speziale, P., Dufrêne, Y. F., Nov. 2016. Mechanical Strength and Inhibition of the *Staphylococcus aureus* Collagen-Binding Protein Cna. mBio 7 (5), e01529–16.
URL http://mbio.asm.org/lookup/doi/10.1128/mBio.01529-16

Hinterdorfer, P., Dufrêne, Y. F., May 2006. Detection and localization of single molecular recognition events using atomic force microscopy. Nature Methods 3 (5), 347–355.
URL http://www.nature.com/doifinder/10.1038/nmeth871

Hutter, J. L., Bechhoefer, J., Jul. 1993. Calibration of atomic-force microscope tips. Review of Scientific Instruments 64 (7), 1868–1873.
URL http://aip.scitation.org/doi/10.1063/1.1143970

JPK, I., 2011. Qi^{TM} mode-quantitative imaging with the nano-wizard 3 afm.

Jørgensen, N., Zobek, N., Dreier, C., Haaber, J., Ingmer, H., Larsen, O., Meyer, R., Sep. 2016. Streptokinase Treatment Reverses Biofilm-Associated Antibiotic Resistance in *Staphylococcus aureus*. Microorganisms 4 (3), 36.
URL http://www.mdpi.com/2076-2607/4/3/36

Kezic, S., O'Regan, G. M., Yau, N., Sandilands, A., Chen, H., Campbell, L. E., Kroboth, K., Watson, R., Rowland, M., Irwin McLean, W. H., Irvine, A. D., Jul. 2011. Levels of filaggrin degradation products are influenced by both filaggrin genotype and atopic dermatitis severity: Natural moisturizing factor levels in atopic dermatitis. Allergy 66 (7), 934–940.
URL http://doi.wiley.com/10.1111/j.1398-9995.2010.02540.x

Kitajima, Y., Jun. 2015. Implications of normal and disordered remodeling dynamics of corneodesmosomes in *stratum corneum*. Dermatologica Sinica 33 (2), 58–63.
URL http://linkinghub.elsevier.com/retrieve/pii/S102781171500035X

Krachler, A. M., Orth, K., May 2013. Targeting the bacteria–host interface: Strategies in anti-adhesion therapy. Virulence 4 (4), 284–294.
URL http://www.tandfonline.com/doi/abs/10.4161/viru.24606

Krishna, S., Miller, L. S., Feb. 2012. Host–pathogen interactions between the skin and *Staphylococcus aureus*. Current Opinion in Microbiology 15 (1), 28–35.
URL http://linkinghub.elsevier.com/retrieve/pii/S136952741100186X

Liu, S., Wang, Y., Mar. 2010. Application of AFM in microbiology: a review. Scanning 32 (2), 61–73.
URL http://doi.wiley.com/10.1002/sca.20173

Mazmanian, S. K., Jul. 1999. *Staphylococcus aureus* Sortase, an Enzyme that Anchors Surface Proteins to the Cell Wall. Science 285 (5428), 760–763.
URL http://www.sciencemag.org/cgi/doi/10.1126/science.285.5428.760

Mulcahy, M. E., Geoghegan, J. A., Monk, I. R., O'Keeffe, K. M., Walsh, E. J., Foster, T. J., McLoughlin, R. M., Dec. 2012. Nasal Colonisation by *Staphylococcus aureus* Depends upon Clumping Factor B Binding to the Squamous Epithelial Cell Envelope Protein Loricrin. PLoS Pathogens 8 (12), e1003092.
URL http://dx.plos.org/10.1371/journal.ppat.1003092

Müller, D. J., Helenius, J., Alsteens, D., Dufrêne, Y. F., Jun. 2009. Force probing surfaces of living cells to molecular resolution. Nature Chemical Biology 5 (6), 383–390.
URL http://www.nature.com/articles/nchembio.181

Nestle, F. O., Di Meglio, P., Qin, J.-Z., Nickoloff, B. J., Oct. 2009. Skin immune sentinels in health and disease. Nature Reviews Immunology 9 (10), 679–691.
URL http://www.nature.com/articles/nri2622

O'Brien, L. M., Walsh, E. J., Massey, R. C., Peacock, S. J., Foster, T. J., Nov. 2002. *Staphylococcus aureus* clumping factor B (ClfB) promotes adherence to human type I cytokeratin 10: implications for nasal colonization. Cellular Microbiology 4 (11), 759–770.
URL http://doi.wiley.com/10.1046/j.1462-5822.2002.00231.x

Oesterhelt, F., Apr. 2000. Unfolding Pathways of Individual Bacteriorhodopsins. Science 288 (5463), 143–146.
URL http://www.sciencemag.org/cgi/doi/10.1126/science.288.5463.143

O'Regan, G. M., Sandilands, A., McLean, W. I., Irvine, A. D., Sep. 2009. Filaggrin in atopic dermatitis. Journal of Allergy and Clinical Immunology 124 (3), R2–R6.
URL http://linkinghub.elsevier.com/retrieve/pii/S0091674909011233

Palmer, C. N. A., Irvine, A. D., Terron-Kwiatkowski, A., Zhao, Y., Liao, H., Lee, S. P., Goudie, D. R., Sandilands, A., Campbell, L. E., Smith, F. J. D., O'Regan, G. M., Watson, R. M., Cecil, J. E., Bale, S. J., Compton, J. G., DiGiovanna, J. J., Fleckman, P., Lewis-Jones, S., Arseculeratne, G., Sergeant, A., Munro, C. S., El Houate, B., McElreavey, K., Halkjaer, L. B., Bisgaard, H., Mukhopadhyay, S., McLean, W. H. I., Apr. 2006. Common loss-of-function variants of the epidermal barrier protein filaggrin are a major predisposing factor for atopic dermatitis. Nature Genetics 38 (4), 441–446.
URL http://www.nature.com/articles/ng1767

Park, H.-Y., Kim, C.-R., Huh, I.-S., Jung, M.-Y., Seo, E.-Y., Park, J.-H., Lee, D.-Y., Yang, J.-M., 2013. *Staphylococcus aureus* Colonization in Acute and Chronic Skin Lesions of Patients with Atopic Dermatitis. Annals of Dermatology 25 (4), 410.
URL https://synapse.koreamed.org/DOIx.php?id=10.5021/ad.2013.25.4.410

Ponnuraj, K., Bowden, M., Davis, S., Gurusiddappa, S., Moore, D., Choe, D., Xu, Y., Hook, M., Narayana, S. V., Oct. 2003. A "dock, lock, and latch" Structural Model for a Staphylococcal Adhesin Binding to Fibrinogen. Cell 115 (2), 217–228.
URL http://linkinghub.elsevier.com/retrieve/pii/S0092867403008092

Que, Y.-A., Moreillon, P., Sep. 2014. *Staphylococcus aureus* (Including Staphylococcal Toxic Shock Syndrome). In: Mandell, Douglas, and Bennett's Principles and Practice of Infectious Diseases. Elsevier Health Sciences, pp. 2237–2271, google-Books-ID: 73pYBAAAQBAJ.

Rankl, C., Zhu, R., Luengo, G. S., Donovan, M., Baghdadli, N., Hinterdorfer, P., Nov. 2010. Detection of corneodesmosin on the surface of *stratum corneum* using atomic force microscopy: Corneodesmosin distribution in *stratum corneum*. Experimental Dermatology 19 (11), 1014–1019.
URL http://doi.wiley.com/10.1111/j.1600-0625.2010.01179.x

Riethmuller, C., McAleer, M. A., Koppes, S. A., Abdayem, R., Franz, J., Haftek, M., Campbell, L. E., MacCallum, S. F., McLean, W. I., Irvine, A. D., Kezic, S., Dec. 2015. Filaggrin breakdown products determine corneocyte conformation in patients with atopic dermatitis. Journal of Allergy and Clinical Immunology 136 (6), 1573–1580.e2.
URL http://linkinghub.elsevier.com/retrieve/pii/S0091674915006491

van Belkum, A., Verkaik, N. J., de Vogel, C. P., Boelens, H. A., Verveer, J., Nouwen, J. L., Verbrugh, H. A., Wertheim, H. F. L., Jun. 2009. Reclassification of *Staphylococcus aureus*

Nasal Carriage Types. The Journal of Infectious Diseases 199 (12), 1820–1826.
URL https://academic.oup.com/jid/article-lookup/doi/10.1086/599119

Vitry, P., Valotteau, C., Feuillie, C., Bernard, S., Alsteens, D., Geoghegan, J. A., Dufrêne, Y. F., Dec. 2017. Force-Induced Strengthening of the Interaction between *Staphylococcus aureus* Clumping Factor B and Loricrin. mBio 8 (6), e01748–17.
URL http://mbio.asm.org/lookup/doi/10.1128/mBio.01748-17

Williams, M. R., Gallo, R. L., Nov. 2015. The Role of the Skin Microbiome in Atopic Dermatitis. Current Allergy and Asthma Reports 15 (11).
URL http://link.springer.com/10.1007/s11882-015-0567-4

Studying the interactions between *Staphylococcus aureus* and atopic dermatitis skin cells using atomic force microscopy

Presented by : Simon Delacroix
Executed in : The Institute of Life Science (Nanobiology group)

Abstract

With the constant increase in the resistance of *Staphylococcus aureus* to antibiotics, it has become a priority to better understand how this pathogen interacts with host tissues, and to develop alternative strategies to fight staphylococcal infections. *S. aureus* plays an important role in atopic dermatitis (AD), a chronic disorder that mostly affects children. Colonization of the skin of AD patients by *S. aureus* exacerbates the disease, and reduced levels of natural moisturizing factor (NMF) in the stratum corneum have been shown to be associated with more severe AD symptoms. Today, two unsolved questions are : i) what are the bacterial adhesins involved in *S. aureus* - skin adhesion, and ii) is the skin protein corneodesmosin (CDSN) a major ligand for *S. aureus* adhesion ? The aim of this master thesis, performed in collaboration with Dr. J. Geoghegan (Trinity College, Dublin), was to use atomic force microscopy (AFM) to study the interaction of *S. aureus* with AD skins, with a particular focus on the above open questions. We first used single-cell force spectroscopy (SCFS) to measure the adhesion forces between different strains of *S. aureus* and AD skin samples with a low NMF level. Using mutant strains of *S. aureus* with deleted adhesins, we have identified the involvement of three major adhesins in the interaction with AD skins : ClfB, FnBPA and FnBPB. In agreement with previous studies, we found that ClfB is responsible for high adhesion forces, $\sim 1600pN$, whereas FnBPs are associated with lower forces $\sim 500pN$. Next we used single molecule force spectroscopy (SMFS) with tips functionalized with an anti-CDSN antibody to detect and map the distribution of CDSN on the surface of AD skins, demonstrating that this protein is more abundant on low NMF skins compared to high NMF skins. Using SCFS, we were also able to partially block the interaction of *S. aureus* with low NMF skin by injecting Fab fragments of the anti-CDSN antibody at increasing concentrations. Both low and high forces were inhibited, suggesting that CDSN might be a ligand for both FnBPs and ClfB on low NMF skins. All together, these results shed new light onto the molecular determinants of *S. aureus*-AD skin interactions : i) ClfB and FnBPs are the main adhesins involved ; ii) the binding strengths of ClfB and FnBPs are high and moderate, respectively, suggesting that two different binding mechanisms are involved ; iii) CDSN seems to be an important ligand for FnBPs, but also for ClfB. Our study opens up new possibilities for the development of anti-adhesive therapies to prevent *S. aureus* from attaching to human skins.

Mots-clés : *S. aureus*, Adhesin, ClfB, FnBP, Skin, Atopic dermatitis, Corneodesmosin